Gel dosimetry for a MR-linac: magnetic field and time dependency

by

Emy van Aert

to obtain the degree of Master of Science
at the Delft University of Technology
to be defended publicly on Tuesday June 2, 2020 at 2:30 PM

Student number:	4738934
Project duration:	August 1, 2019 - June 2, 2020
Supervisors:	Dr.Ir. Antonia Denkova
	Dr.Ir. Jochem Wolthaus
	Simon Woodings BSc
Thesis committee:	Dr.Ir. Antonia Denkova
	Dr.Ir. Dennis Schaart
	Dr. Kristina Djanashvili

1 Preface

This master started for me in September 2017. After two years of working as a Medical Physics Engineer at UMC Utrecht I decided to go back to university to obtain my MSc degree. It were a busy three years, while combining work and study, but I'm happy I did it. There are a lot of people who I need to thank for this. First of all, Erik. Erik made it possible for me to spend almost all my time on my study and my work, and less time with him and our household... Besides Erik, also all my colleagues deserve a big thank you, especially my fellow Medical Physics Engineers. They accepted my very strange working hours during the first two years and took over my tasks during my graduation project and internship. I'm very grateful to the UMC Utrecht and Jack that I got the opportunity to do this. Last, but definitely not least, I would like to thank Jochem, Simon and Antonia for supervising me on this project.

2 Abstract

The goal of this research was to perform a 3D end-to-end test on a MR-linac to check the whole workflow using a clinical treatment plan. Dosimetric gel was used to obtain 3D spatial information, with the phantom in the same position for irradiation and scanning. In order to achieve this, fundamental elements of gel dosimetry needed to be investigated. In the MR-linac, irradiation is delivered in the presence of a permanent magnetic field. Therefore, the dosimetric response within a 1.5 T magnetic field should be validated. It is also important to investigate the time-dependence of the gel. It is preferable to read-out the gels within approximately one hour, so that the phantom does not have to be moved. Ideally, scanning and irradiation would be done at the same time, to see the dynamical dose delivery. The VIPAR gel was used for this research.

The experiments demonstrated that R2 values for doses irradiated with magnetic field were the same as R2 values for the same dose irradiated without magnetic field. R2 values are still proportional to the dose. It was also shown that it is possible to scan the phantom within 20 minutes after irradiation. Sensitivity is at its highest after approximately 8 hours and stays stable afterwards, so scanning after 8 hours will improve the read-out accuracy. It was also possible to make a fit for the R2 versus time plots, which makes it possible to correct for change over time. The fit can be divided in two linear parts if time is plotted on a logarithmic scale, one fit for the time points before 7 hours, one for the time points after 7 hours. The partial doses acquired by the gel during radiation delivery were estimated. The equivalent R2 values then agreed with the extrapolated fit to within 4%. This is a good indication that dynamic gel (4D) dosimetry may be achievable.

A protocol for a relative end-to-end test was also developed. From the preliminary results, it appeared that a relative end-to-end test can be performed with the read-out of gel within 1 hour. A new MR sequence needs to be developed. For this end-to-end test, the sequence needs to scan a larger volume with a higher resolution, therefore, the scan time will increase and real-time dosimetry will not be possible. Changing the MR sequence might also change the optimal irradiation-scanning interval and the R2 versus time curve. To perform absolute dosimetry, an extra calibration would be required.

Contents

3 Introduction

Radiotherapy is an important option for cancer treatment. In 2018, there were 116.537 new incidences of cancer in the Netherlands [1]. More than half of the patients receives radiotherapy [2]. In external beam radiotherapy (EBRT) a high energy megavoltage photon beam is generated and aimed at the tumor. To deliver the right dose to the tumor while minimizing dose to the surrounding tissue is a very complex process. Before start of the treatment, patients are imaged with computed tomography (CT) or magnetic resonance imaging (MRI). A treatment planning system (TPS) is used to create a treatment plan on this CT or MR, which is sent to the linear accelerator (linac). The treatment plan contains information about field shapes, dose rates, gantry angles and many more parameters. To assure that the planned dose is also the dose given to the patient, quality assurance (QA) is performed. QA is done for every part of the process.

Different measurement methods can be used to perform plan QA. Probably the most simple QA measurement is to perform a point measurement with an ionization chamber. This measurement checks whether the recorded dose in the chamber is the expected dose in the volume. It only says something about one point. 2D measurements can be done using ionization chamber arrays, diode arrays, electronic portal imaging devices (EPIDs) and radiochromic film [3]. These methods can be used for relative or absolute measurements. For absolute measurements, a calibration is required. A disadvantage of these measurements is that they only give information on one point or one plane. 3D measurement methods can be used to provide information about the whole dose distribution. Examples of 3D measurement methods are 3D gels and PRESAGE dosimeters [4] [5] [6]. Those methods are not yet widely available and more research needs to be done.

Since 2017, patients are also treated with MR-linacs. A MR-linac is a combination of a linac with a 1.5 T MRI system. This thesis will be about the use of gels for dosimetry in a MR-linac system [7]. There are multiple questions which still need to be addressed. The first part of this master thesis will be about whether the magnetic field has an influence on the behavior of the gel. The second part will focus on the behavior of the gel over time. The last part considers using the gel for 3D dosimetry of treatment plans and end-to-end testing.

3.1 Gel dosimetry

Gel dosimetry was first introduced in the 1950s [8]. Since then, a lot of work has been done, but it is still mostly research. The first gel dosimeter used was the Fricke dosimeter, which was read-out via spectrophotometry. Gore was then the first (in 1984) to use magnetic resonance imaging (MRI) to create a three dimensional radiation dosimetry system. They showed that the T1 relaxation parameter varies proportionally with the dose [9]. After Fricke dosimeters, gel dosimeters consisting of polymers were made. Polymer gel dosimeters are made from radiation sensitive chemicals which form a polymer after irradiation. Polymer gels are hydrogels in which monomers are dissolved. Radicals created in the irradiation of water induce the polymerization of the monomers. This takes place as a function of the absorbed radiation dose. The purpose of the gel matrix is to hold to polymer in place, in order to preserve spatial function.

Various gelling agents can be used to form the gel, for example gelatin, agarose, sephadex and polyvinyl alcohol [10]. The polymer chains then bind water protons more tightly, which causes the paramagnetic properties to change [11]. For those polymer gels, the reciprocal of T2, or R2, relaxation rate, is proportional to the dose given [12]. Further developments were aimed at creating polymer gels that were less toxic and had a higher sensitivity. Polymer gels overcome some of the disadvantages of conventional, point-based dosimeters. Such disadvantages are tissue non-equivalence, radiation beam perturbation and energy and/or dose rate dependent response [13]. A disadvantage of the gels is that their response is inhibited by the presence of oxygen. For this, normoxic gel dosimeters were developed. For example ascorbic acid is used in those gels to bind the oxygen [14].

For different gel compositions, there are different ways to read-out the gels. For some gels, measurements of optical density are possible, for other gels the change in attenuation coefficient can be measured with x-rays. Ultrasound can be used if polymerization leads to changes in elasticity. Vibrational spectroscopy can be used to show the change from monomers to polymer chains [6]. Another way to read-out gels is to use magnetic resonance imaging (MRI). The readout methods will be more extensively described in section 3.1.3..

Gel dosimetry can be used for multiple purposes in radiotherapy. It can be used for patient or linac QA. Basic dosimetry can be done like percent depth doses (PDD) and beam profile measurements, but also more complicated dose distributions in external beam therapy. The gels can also be used for brachytherapy or proton therapy or to determine the dose of imaging procedures from for example, CT imaging. The effect of tissue heterogenities, like bone and air, can also be assessed with gel dosimetry [6] [15].

3.1.1 Different types of gels

As said above, the first gel dosimeter developed was the Fricke gel dosimeter. The Fricke dosimeter consists of a ferrous sulphate solution [16]. The basis of the Fricke dosimeter is the transformation of ferrous (Fe^{2+}) to ferric (Fe^{3+}) ions [16]. This transformation is dose dependent, so the concentration of ferric ions is proportional to the radiation dose [17]. Advantages of the Fricke dosimeter are that it can easily be prepared and it is possible to determine the spatial dose distribution shortly after irradiation [17]. The gel is also tissue equivalent. However, a disadvantage of Fricke dosimeters is that the ferric ions produced by absorption of radiation diffuse through the gel, which leads to a decrease in signal intensity and destroys the spatial dose information [6] [17]. The absorbance of radiation is stable between 20 and 60 minutes after irradiation, the readout has to be done in this period. The Fricke dosimeter is independent of dose rate and photon energy and linear in the range of 1-15 Gy [18]. The dosimetric properties can change with gel preparation and measurement conditions [17]. It is therefore very important to have a strict local protocol for the gel preparation and measurement conditions.

In 1954, Alexander et al published the first article about the use of polymer gels for radiation dosimetry. The size of the polymers reduces diffusion. They used polymethylmethacrylate [19]. Later, polymerization in liquids was investigated, as well as the use of polyacrylamide as a gamma dosimeter [20] [21]. In 1992 a new gel formulation was proposed, consisting of acrylamide (AAm)

and N,N'-methylene-bis-acrylamide (Bis) in an aqueous agarose matrix. This gel was given the name BANANA. The BANANA polymer gel did not have the diffusion problems from the Fricke dosimeter. It was also quite stable after irradiation [22]. Later, the agarose was replaced with gelatin, which was named BANG (consisting of Bis, AAm, nitrogen and aqueous gelatin). This polymer gel was patented and became commercially available [23]. Other, non-patented gels with polyacrylamide are called PAG-gels [10] [24]. The polymer type gel dosimeters do not have the diffusion problem of the Fricke dosimeters, but they do have the problem that oxygen inhibits the polymerization process. Because of this, the polymers have to be made in an oxygen-free environment [25]. Those polymers are also called hypoxic or anoxic [10]. This led to the development of the MAGIC gel dosimeter. In the MAGIC dosimeter, oxygen is bound in a metallo-organic complex, which removes the problem of oxygen inhibiting polymerization. Ascorbic acid, also known as vitamin C, binds the free oxygen into the metallo-organic complexes. It is also possible to use other antioxidants. These dosimeters are so called normoxic dosimeters [26].

In 1999, Pappas et al developed a N-vinylpyrrolidone argon (VIPAR) gel. The gel consists of N-vinylpyrrolidone, N,N'-methylene-bisacrylamide, gelatin type A and water. The VIPAR gel is an hypoxic gel, where argon is used to remove oxygen. They showed that the gels relaxation rate R2 is linearly related to dose with a dose sensitivity that remains stable over time, measured on day 4, 5 and 15 after irradiation. They also showed good reproducibility of results [27]. The VIPAR gel is the gel that will be used for this project.

3.1.2 Working mechanism of polymer gels

Polymer gels consist for the majority of water. VIPAR gels contain 87% water [27]. When water is irradiated, water molecules dissociate into multiple highly reactive radicals and ions. This process is called radiolysis. This reaction is shown in equation 1, where $R^{\bullet}$ is the radical. How often this reaction takes place is proportional to the absorbed dose.

$$H_2O \rightarrow 2R^{\bullet} \tag{1}$$

The radicals which are formed in this reaction then start the polymerization of the monomers by the following reaction, where M_m is the monomer.

$$R^{\bullet} + M_m \rightarrow M_m^{\bullet} \tag{2}$$

The polymer chain then grows further by chain propagation reactions by adding monomers or adding vinyl groups of other polymer chains. This reaction is shown in equation 3, where M_m is the monomer and M_n is a polymer with n monomer units.

$$M_m^{\bullet} + M_n \rightarrow M_{n+1}^{\bullet} \tag{3}$$

Termination of the polymerization reaction happens when two radicals react. In this case, one large polymer can originate, or two separate polymers. The reaction can also be ended by the reaction of a polymer with a radical that

arised in the radiolysis reaction. Those reactions are shown in equations 4, 5 and 6.

$$M_m^\bullet + M_n^\bullet \rightarrow M_{n+1} \tag{4}$$

$$M_m^\bullet + M_n^\bullet \rightarrow M_m + M_n \tag{5}$$

$$R^\bullet + M_n^\bullet \rightarrow M_n \tag{6}$$

It is also possible for the radicals of the radiolysis reaction to start polymerization again for a dormant polymer chain. This reaction is shown in equation 7. It is also possible for the radical to be transferred to other molecules. This is shown in equation 8 [10].

$$R^\bullet + M_n \rightarrow M_n^\bullet \tag{7}$$

$$M_m^\bullet + M_n \rightarrow M_m + M_n^\bullet \tag{8}$$

In summary, the degree of radiolysis is proportional to the absorbed dose. The degree of radiolysis determines the degree of polymerization, so the degree of polymerization is also proportional to the absorbed dose. The degree of polymerization influences material properties, for example density, optical density, the attenuation coefficient, speed of propagation of sound and proton mobility. All those properties can be used to read-out the gels.

3.1.3 Readout of gels

Optical CT, X-ray CT, ultrasound, vibrational spectroscopy and MRI can be used to read-out the gels.

Optical CT Scanning the gels with optical computed tomography (CT) is based on the principle that the optical density of the gel increases with dose. Unirradiated, the gels are transparant to visible light. Upon irradiation, the gels turn opaque, but remain translucent enough to be able to use optical CT. A monochromatic light beam goes through the gel and is attenuated by the gel. From the measured intensity of the exit beam, the attenuation μ can be calculated. This attenuation is correlated to the dose received by the gel. The CT principle works the same as X-ray CT: a planar image is made from a series of line integrals. Multiple planar images are back-projected to an image [28] [29].

X-ray CT X-ray CT uses X-rays instead of light to create the images. CT images are a visualization of Hounsfield Units (HU). The Hounsfield unit for a certain material is given by formula 9:

$$HU = 1000 * \frac{\mu - \mu_w}{\mu_w} \tag{9}$$

With this formula, the linear attenuation coefficient (μ) can be calculated, which is correlated to dose. Polymerization of the gel causes the density to increase. The linear attenuation coefficient changes because of a change in density. The increase in density is related to a decrease in volume, but it was shown that the increase in density is not more than 1% for a fully polymerized polymer [30].

Ultrasound (Medical) Ultrasound is a diagnostic imaging technique which uses sound waves to create images. With ultrasound, a number of parameters can be measured. These parameters give information about the characteristics of a material. Most commonly measured are ultrasonic speeds of propagation, attenuation and reflection coefficients. Acoustic speed is influenced by the elastic modulus and density. The density of polymer gels increases with irradiation and the formation of polymer chains might also increase the rigidity and thereby the elastic modulus. In this way, the acoustic speed can be used to read-out gels. The attenuation and transmitted intensity also correlate to absorbed dose. The acoustic speed of propagation can be measured with the highest precision, and is therefore the most useful parameter to measure [31].

Vibrational/Raman spectroscopy Raman spectroscopy makes use of Raman scattering. If a monochromatic beam of photons interacts with a transparent medium, a part of the photons is scattered by Rayleigh and Raman scattering. Raman scattering is an inelastic process. The change in energy of the measured photon corresponds to the energy levels of the various molecular vibrations. Those energy levels change with copolymerization and cross-linking, which makes it possible to use Raman spectroscopy for read-out of polymer gels [32].

MRI MRI creates images based on the relaxation of protons. On a MRI, T1 and T2 weighted images can be made. For T1, the magnetization is flipped to the transverse plane. The magnetization will grow back along the direction of the static field. The T1 time of a material is the time it takes to recover to 63% of the equilibrium magnetization M_0. Besides T1, there is another relaxation effect: the dephasing of spins in the transverse plane. The T2 or spin-spin relaxation time is the time after which M_xy is 37% of M_0 [33]. From T1 and T2, relaxation rates R1 and R2 can be calculated with $R1 = 1/T1$ and $R2 = 1/T2$. For gel dosimetry read-out, R2 is most used. When the gel dosimeters are irradiated, the molecular mobility is significantly reduced. When the mobility of the water is reduced, spin-spin relaxation is more effective, which is seen in a decrease in T2. This means an increase in R2 [10].

3.1.4 Dosimeter characteristics

Polymer gels have a few characteristics to take into consideration when using polymer gels for dosimetry.

Time influence Deene et al showed in 2000 that there are two processes which influence the stability of the R2 of the gel. The first one is post-irradiation polymerization, which lasts until about 12 hours after irradiation. The second one is the ongoing gelation of the gelatin in the gel. This process continues

for more than a month [34]. Papoutsaki et al also showed that the offset of R_0 increases and the sensitivity decreases over time [35]. They also investigated the optimal time between gel manufacturing and irradiation. This interval should not be more than 7 days. For the time between irradiation and MR scanning, they found that the sensitivity increases after irradiation. There is a maximum around three weeks, after which the sensitivity stabilizes at a little bit lower value. The sensitivity is the steepness of the slope of the R2 versus dose plot.

Dose rate and fractionation influence For different gels, dose rate dependencies were found. This dose rate dependency is very gel-type dependent. For example, the PAG dosimeter has a small dose rate dependence, whereas the nMAG dosimeter has a much larger dose rate dependency [36]. Dose rate dependence was investigated for the $VIPAR^{CT}$ (or VIC) gel. This gel is comparable to the VIPAR gel used. They tested different dose rates between 1.047 and 6.282 Gy/min. They showed no dose rate influence [37]. The fractionation dependence was not studied extensively for VIPAR gels. There were some experiments with a boost irradiation on a gel irradiated before, much later than the first irradiation, which showed no difference. This implies that there is no dose rate effect for VIPAR gels [27].

Temperature influence There is a temperature dependence during irradiation as well as during scanning. The temperature dependence during irradiation is not studied for VIPAR gels, but a change in sensitivity was found for PAG and nMAG gels. Especially if the temperature gets to the melting point of the gel, the sensitivity gets worse. There is also a temperature dependence during scanning. This temperature dependence might lead to another R2 versus dose curve, which causes problems if you want to do absolute dose measurements [36]. For relative measurements, this is not a problem. For BANG gels, it was shown that the temperature dependence is caused by water molecules rotating more rapidly with higher temperatures. Since VIPAR and other polymer gels consist also for the majority of water, it is likely that there is also a temperature dependency for VIPAR gels [38]. For the VIPAR gels, it was advised to irradiate and store them at room temperature.

Influence of radiation source and energy Pappas et al investigated in 2003 the influence of using different photon energies and whether there was a difference between photon and electron beams for VIPAR gels. They did relative dose measurements for 6 and 23 MV photon and 6, 9, 12, 15 and 18 MeV electron beams. The measurements were also compared with ion chamber relative measurements. A good agreement between gel data en corresponding ion chamber measurements was seen. They concluded that it is possible to do relative dose measurements for those beams and energies without the need for a calibration curve [40].

3.2 Gel dosimetry for regular linacs

The gel used for this thesis is the VIPAR gel. In 2001, Pappas et al showed that this gel can be used for beam profile measurements [39]. They used the polymer gel, radiographic film and a PinPoint chamber for profile measurements

of a 6 MV beam with a 5 and 10 mm diameter. The penumbras measured with the polymer gel were smaller than the penumbras measured with film or the PinPoint chamber. This is caused by the finite size of the conventional detectors. The relative depth dose measurements showed good correspondence between film and gel. They concluded that using the polymer gel can deliver relatively accurate profile data for small beams. Kipouros et al also showed that the gels have a linear response up to 42 Gy [13]. They also did an experiment with an ^{192}Ir brachytherapy source up to 250 Gy. This curve can be fitted with a logarithmic fit. This makes it possible to use the gel to verify clinical doses, which are up to 24 Gy/fraction.

In more recent years, research was done using the VIPAR gel for plan verification. Saenz et al created two 3D printed phantoms of a patient with a lesion in the lumbar spine [41]. One phantom was filled with gel, the other phantom had two openings for ionization chambers. Pre-treatment QA on a detector array was also performed. The gamma analysis of the detector array showed 95.4% of the points passing for 3%/2mm criteria. The ionization chamber measurement was within 3% of the calculated dose, for the target as well as for the spinal cord. The 3D gel phantom dose distribution showed 97% gamma passing rate using 3%/2mm. This showed that it is possible to verify dose and spatial accuracy with gel dosimetry. In 2016, Liu et al also used the VIPAR polymer gel to validate automatic treatment planning software for brain metastases [42]. The validation used ionization chamber measurements, diode array measurements (Delta4) and a patient-specific 3D phantom filled with gel. The three methods showed good correspondence.

3.3 Gel dosimetry in a MR-linac

An MR-linac is an integrated 1.5 T MRI and accelerator. It is one of the newest developments in image guided radiotherapy (IGRT). The MR-linac can be used for on-line, soft-tissue based position verification and treatment monitoring [43]. When radiation is delivered in a MR-linac, there is a constant magnetic field. This magnetic field influences the dose distribution, but might also influence the behavior of the gel.

3.3.1 Influence of magnetic field on beam

The Lorentz force caused by the magnetic field influences the secondary electrons. The secondary electrons have a helical path between two collisions, which results in a smaller build-up distance and a slightly shifted and asymmetrical penumbra. This helical path also leads to the Electron Return Effect (ERE). Electrons entering air have this helical path, which causes them to return back into the phantom or patient, this is schematically shown in figure 1. This leads to extra dose deposition. This effect is seen for the transition from phantom to air, so also in air cavities inside the phantom [43] [44]. This effect is shown in simulations, but also on film [43]. At boundaries to a high-density material there is a dose decrease [45]. The ERE is field strength dependent. Raaijmakers et al investigated the ERE for field strengths of 0.2, 0.75, 1.5 and 3 T [45]. They saw different effects for different magnet strengths, depending on field size and the side of the beam (lateral or distal). The size of the air cavity also plays an important role. The ERE only adds dose if the cavity is bigger than the size of

the helical trajectory of the electrons, otherwise the electrons will not return to the exit point, but they will re-enter the phantom or patient at another point.

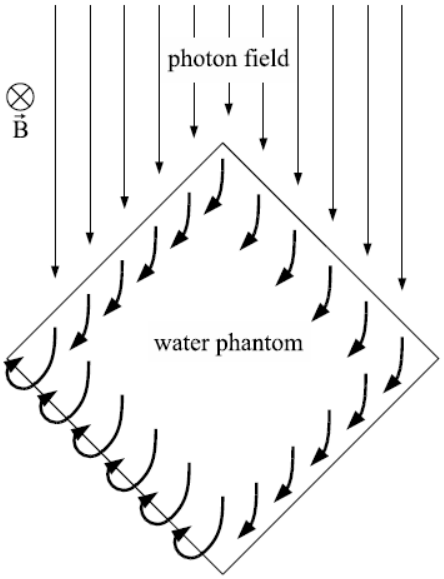

Figure 1: A schematic representation of the ERE in a magnetic field. [46]

3.3.2 Influence of magnetic field on gel behavior

There is little research available about how gels behave in a magnetic field. There are some recent publications in which the influence of the magnetic field is investigated. In 2018, Lee et al published an article about the use of iron-based radiochromic 3D gels [47]. They used a 1.5 T, 7 MV MR-Linac with Fricke-type dosimeters to perform real-time 3D dosimetry. Fricke gels have the known diffusion problem, but since now it is possible to scan and irradiate at the same time, this problem is reduced. They irradiated 4 different gels with constant dose rate: ferrous oxide xylenol orange (FOX), ferrous chloride xylenol orange (FCX), ferrous phthalocyanine xylenol orange (FPX) and Fricke xylenol orange gel (FXG). The difference in the gels is in the iron compounds. They showed that for FOX, FCX and FXG the real-time relative MR signal was linear with time, and therefore dose. This shows that the conversion of ferrous (Fe2+) to ferric (Fe3+) ions happens quick enough to make real-time MR imaging possible. From those four gels, the FOX gel was the most suitable gel for MR-IGRT studies, because it had the highest signal intensity. They also showed that the MR signal intensity stayed constant for at least 20 minutes after irradiation. They did not make a comparison with gels irradiated without the presence of a magnetic field.

Roed et al published an article in 2019 about the use of the BANG3-Pro polymer in combination with a 1.5 T magnetic field [48]. They investigated dose response, dose-rate dependence and fractionation dependence. The dose response was investigated by irradiating five gel dosimeters in a phantom to different doses with a regular linac, with and without a 1.04 T magnetic field.

The field was generated by an electromagnet. The dose rate dependence was tested by extending the distance between the source and the dosimeter. This led to dose rates of approximately 450 cGy/min (100%) and 63 cGy/min (14%). The fractionation dependence was explored by delivering a dose of 10 Gy in 1 fraction and in 3 fractions of 3.33 Gy with 9 minutes in between. They also did an end-to-end test with a spherical gel dosimeter. The results showed a linear dose response with the same slope for the beams with magnetic field and without magnetic field. For the dose rate dependence they showed that there is a dose rate dependence, but it does not change with magnetic field. The same goes for the fractionation dependence. The end-to-end phantom study dose distribution had a gamma pass rate of 85.6%, which was less than expected. It was seen that the gamma analysis failed at beam entrance and beam exit regions. This might be due to the high dose rate dependence. They concluded that using the gel as a 3D dosimeter for end-to-end testing needs more research.

Pappas et al looked at 2D and 3D dosimetry for the Elekta Unity MR-linac in 2019 [35]. They used two identical 3D-printed head phantoms. One phantom was filled with polymer VIPAR gel, the other phantom had a film insert. They showed that 2D and 3D measurements corresponded well with the calculated dose distributions. They did not irradiate the phantoms with the same plan on a linac without magnetic field, so it is not possible to conclude that the magnetic field has no influence.

3.4 End-to-end testing

An end-to-end test is performed to check all aspects of the treatment procedure. The whole treatment chain is checked, including imaging, treatment planning, positioning, treatment plan adaptation and accurate dose delivery. For this, multiple measurement methods can be used, including ionization chambers, TLDs, film and gel. Also, different phantoms can be used. The end-to-end test for regular linacs starts with a CT of the phantom. Afterwards, the CT is transferred to the TPS where a treatment plan is created. The next step is to align the phantom at the linac. This step might also include imaging of the phantom with cone beam CT (CBCT) to verify the alignment. The table is then moved to shift the phantom to the right spot. After this, treatment is delivered and the measurements can be analyzed. The dose measured is compared to the dose of the treatment plan [49] [50].

End-to-end tests for MR-linacs have some changes and some additional tests to test the whole workflow. The first step is still a CT, which is used to create a treatment plan. The next step is a pre-treatment MR scan, which is used to adapt the delineations. A new adapted plan is created afterwards. This plan is then delivered. It is also possible to partially deliver the plan, move the phantom, make a new MR scan and a new partial plan. After the irradiation, the measurements are analyzed again [51] [52]. With a MR-linac, it is possible to scan and irradiate at the same time. That makes it also possible to irradiate the polymer gels and scan at the same time. This means that it would be possible to follow the dose build up during irradiation.

3.5 Research questions and hypotheses

The end goal of this thesis work is to perform a 3D end-to-end test with a gel dosimeter on a MR-linac. In order to achieve this, elements of the performance of the gel in a 1.5 T magnetic field were investigated.

3.5.1 Research question 1: Gel dosimetry in a magnetic field

The first question that needs to be answered is how the gel behaves when a magnetic field is present. There are two subquestions.
1) Is the R2 still linear with dose if a magnetic field is present?
2) Is there a difference between vials irradiated in a magnetic field and vials irradiated without magnetic field?
Hypothesis is that the presence of a strong magnetic field does not affect the dose response of a VIPAR polymer gel. Thus, as previously demonstrated for conventional radiotherapy dosimetry, the T2 relaxation rate (R2) is expected to remain proportional to the dose delivered. This will be investigated for a range of different magnetic field strengths. If this is proven, it will imply that gel dosimetry in an MR-linac is achievable with minimal modification to conventional gel dosimetry protocols.

3.5.2 Research question 2: Time dependency of gel dosimetry

The second question is how the gel behaves over time. There are a few subquestions:
1) What is the trend over time or variation for the gel and is it possible to model this?
2) When would be the best moment to scan the gel? Would it be possible to scan the gel within one hour?
3) Is it possible to scan and irradiate at the same time, how precise can the dose be determined?
To answer this research question, experiment 2 was performed.
Hypotheses were that the R2 readout of a VIPAR gel varies with time, but that the variation can be modelled as a function of dose and time. The best moment to scan the gel would be between 1 day and three weeks after irradiation. Scanning and irradiating at the same time might be possible, but will come at an accuracy cost. The readout variation will be characterized over a time period from during and immediately after exposure, up to 43 days post-exposure.

3.5.3 Research question 3: End-to-end test

The third question is whether it is possible to use a polymer gel phantom to do a 3D end-to-end test on a MR-linac. Hypothesis is that VIPAR gel can be used to perform a 3D relative-dose end-to-end test in a MR-linac. It is intended that the test be sufficiently accurate to perform a meaningful gamma analysis with 3% dose / 3 mm parameters and with a low dose threshold of 10%. A protocol describing the end-to-end test will be established. The potential for real-time 4D dosimetry will be considered.

4 Experiment 1 - MR field dependency of VIPAR gels

4.1 Goal and outline of experiment

The first experiment was conducted to answer the first research question: How does the VIPAR gel behave in the presence of a magnetic field? Hypothesis was that the presence of a strong magnetic field does not affect the dose response of a VIPAR polymer gel. The relationship between R2 and dose needs to be known in order to do relative or absolute dosimetry. The magnetic field dependency needs to be determined in order to do dosimetry at a MR-linac.

In this experiment, VIPAR gels were irradiated up to 8 Gy while experiencing magnetic field strengths up to 1.47 T. This was achieved with a Bruker magnet and a conventional linac modified to deliver a flattening filter free (FFF) beam. Section 4.2 describes the preparations of equipment needed for this. Section 4.3 gives a description about the methods and materials. Section 4.4 shows the results of the experiment, which are discussed in section 4.5. Section 4.6 gives the conclusions.

4.2 Preparation

Installing the FFF beam The first experiments were done on an Elekta Synergy linac (U4) (Elekta, Crawley United Kingdom) that was suitable for clinical use, but used exclusively for research. This machine had X-ray energies of 6, 10 and 18 MV (X6, X10, X18) and electron energies of 6, 8, 12, 15 and 18 MeV (E6, E8, E12, E15 and E18). The X-ray energies all had a flattening filter to flatten the beam. They are so called flattening filter (FF) beams. The advantage of FFF beams for this experiment is that the dose rate is three times as high as for a FF beam. Since irradiation for this experiment took place at extended distance (3 meters) from the gantry head, the dose rate was low. In order to increase this, a FFF beam was used. Since this was not yet available, FFF was installed on the U4.

Installation of FFF on the U4 consisted of two parts, a hardware part and a software part. The hardware part was done first. The first step was to remove the filter. Instead of a cone shaped filter, a thin steel plate was inserted in front of the beam to stop scattering. By removing the filter, the dose rate was increased due to reduced attenuation. Removing the flattening filter also changed the shape of the beam profile. In figure 2 beam profiles for a FF and a FFF beam are shown. The steel plate scatter filter was custom-made. Inside the head of the linac is a filter carousel with five slots which where all used for existing beams. The 18 MeV electron scattering filter was removed to make space for the FFF beam and filter (see figure 3). The printed circuit boards controlling dose rate were also upgraded.

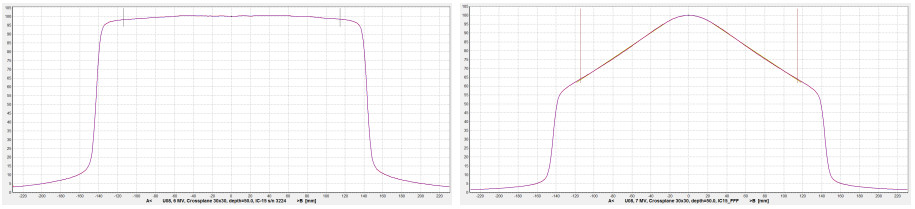

(a) (b)

Figure 2: (a) A beam profile of a beam with flattening filter showing a flattened field (b) A beam profile of a beam without flattening filter showing the non-uniform dose distribution across the field. The X-axis shows the position from the isocenter, the Y-axis shows the relative dose, normalized at the center of the field. Both fields have field size 30x30 cm^2.

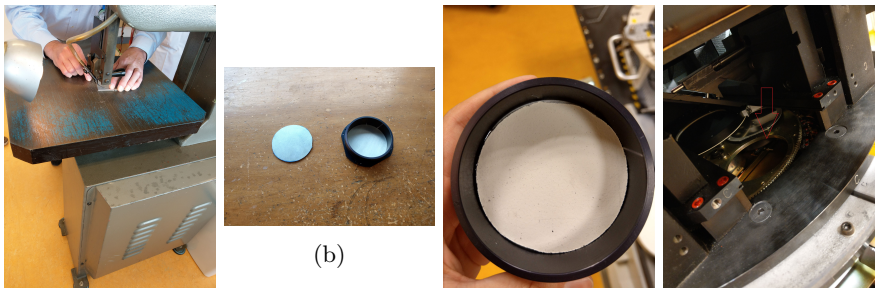

(a) (b) (c) (d)

Figure 3: Photos of the preparations of the U4. (a) Sawing of the steel plate scatter filter. (b) The steel plate and the filter. (c) The steel plate in the filter. (d) The filter carousel where the filter is placed.

The software also required adaptations in order to accommodate the new energy. The software supports only three photon energies. Therefore, the new 6 MV FFF beam replaced the 18 MV photon beam. After the adaptations, the U4 had photon energies of 6 and 10 MV FF, 6 MV FFF and electron energies of 6, 8, 12 and 15 MeV.

After this, it was necessary to set up the FFF beam parameters. The energy of the FFF beam of the U4 was matched to the energy of the clinical FFF beams. The magnetron power was increased to get the right dose rate and energy. In order to create a photon beam, electrons are ejected from the gun at the beginning of the waveguide and then accelerated until they hit the (high Z) target and produce bremsstrahlung photons [53]. The electrons are steered, focussed and bend by a set of magnets around the waveguide. This determines the direction and angle of the produced beam. An overview of the steering magnets is shown in figure 4. The 1T, 2R and bending magnets mainly influence the inline direction (parallel to the waveguide), whereas the 1R and 2T steering magnets mainly influence the crossline direction (perpendicular to the waveguide). Besides the bending and steering magnets, there are also focus magnets which are in place to focus the beam. They are at the beginning of the waveguide. The ion chamber registers the fluence of the beam after the

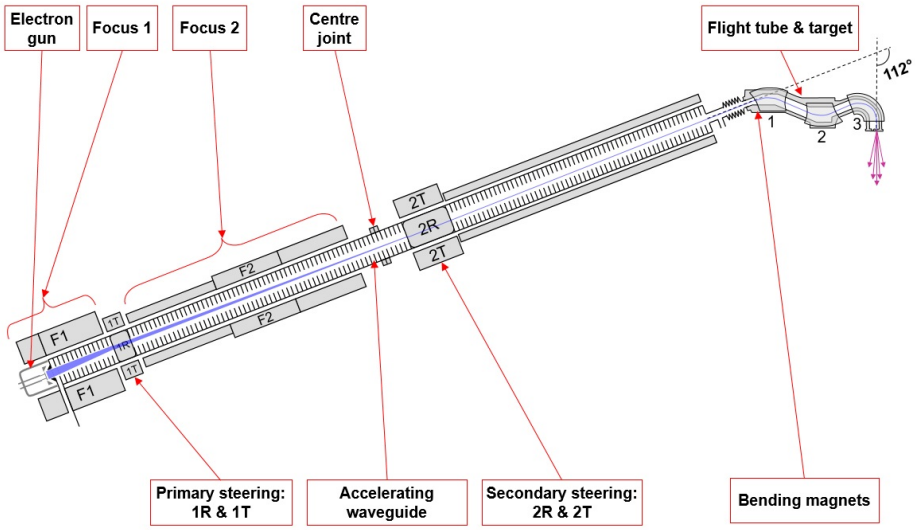

Figure 4: Schematic overview of the steering of a linac. The primary steering and focus coils are at the start of the waveguide, followed by the secondary steering coils. The steering influences the profile of the beam. Figure courtesy of Elekta.

target. When the ion chamber measures a field that is not symmetric, the servo mechanism is triggered and the 2R and/or 2T currents are adjusted. There is also a gantry angle dependent correction for the Earth's magnetic field, which is in the Look Up Table (LUT). The combination of the set currents for the primary and secondary steering, the LUT and the servo mechanism determine the beam profile.

To determine the optimal 1R and 1T currents, two ionization chambers were placed directly behind the 1R and 1T magnets at the waveguide. If the steering is optimal, the electron beam passes smoothly through the waveguide. Few electrons hit the walls, and measured scatter will be minimized. The measurements are shown in figure 5. Two ionization chambers were used to ensure consistency, which was observed. The measurement could also be done using only one ionization chamber.

From this experiment it was concluded that optimal values for 1R and 1T were 0 and 28 mA. It was then necessary to find the optimal 2R, 2T (secondary steering) and bending currents. Those were determined using a Starcheck (Starcheck Maxi, PTW, Freiberg, Germany) and tuning the 2R and 2T currents to achieve maximum dose rate. The Starcheck is a 2D ionization chamber array which can be used to measure beam profiles. The center and beam peak of the FFF beam have to be at the same location as the center of the X6 FF beam. This was performed at gantry 0 degrees. After tuning, all profiles and PDDs were also checked in a water tank.

The X6 FFF has a different energy than the previous X18, and additionally because the Bruker magnet was placed next to the linac, a new LUT had to be made. Generally, the LUT corrects for the changes in the Earth's magnetic

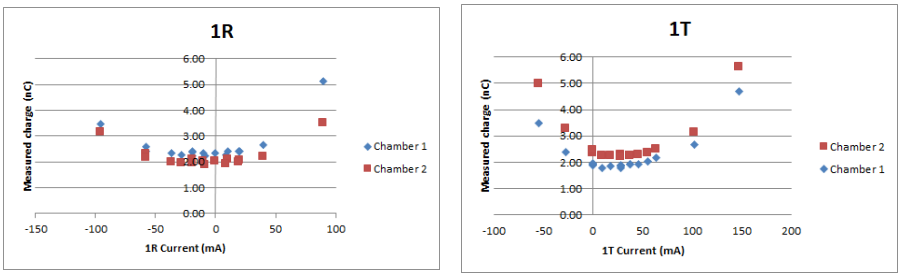

(a) (b)

Figure 5: Results of the experiment with the ionization chamber on the waveguide. (a) Shows the results for the 1R current, (b) Shows the results for the 1T current. Optimal current is where the scatter is the least, so around 0 for 1R and around 28 for 1T.

field for different gantry angles. Since the Bruker electro magnet has an intrinsic magnetic field, the magnet influenced the magnetic field around the linac. In figure 6 a plot is shown of the 2T linac error for the new and the old LUT in the crossline direction. The same was done for the inline direction. The 2T linac error is defined as the field symmetry metric measured by the ionization chamber in the crossline direction. To determine the symmetry, two dose points that are equidistant from the central axis are compared. A clear decrease in error was seen. A linac error of 5 corresponds to a symmetry error of 5%, which for FFF is also equivalent to a displacement of the field edges or beam peak of approximately 1 mm.

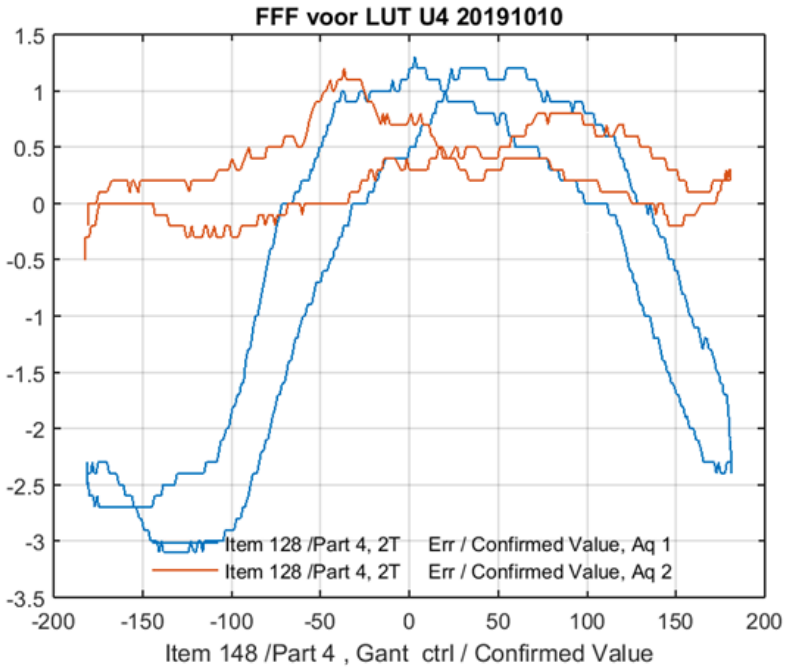

Figure 6: Plot of the 2T linac symmetry percentage error versus gantry angle. The blue line shows the error for the old LUT, the red line shows the error for the new LUT. Plots are made with the linac servo off. The new LUT improved the linac error.

After this, the field symmetry and energy were checked throughout 360 degrees with the Starcheck attached to the head of the linac. The resuls were within clinical tolerances. Subsequently, starshot tests were performed that measures the isocentric alignment of the beam. A gafchromic film was irradiated with beams from multiple gantry angles. The diameter of the smallest sphere containing all beams describes the position of the isocenter. This resulted in a radius of 0.18 mm for the clockwise rotation and 0.10 mm for the counter-clockwise rotation. Clinical tolerance is 0.5 mm for high-accuracy stereotactic linacs.

Influence of the magnet With the beam well-adjusted for the normal 0 T magnetic field, it was then necessary to check its performance over range of magnetic field strenghts used in the experiment. Ten discrete magnetic field strengths were available, ranging from 0 to 1.5 T. These were checked with a Sypris 5180 Gauss/Tesla meter. Results are shown in table 1.

Table 1: Measured magnetic field for each set magnetic field strength. There is a good agreement between set and measured magnetic field strength.

Set magnet strength (T)	0	0.15	0.3	0.45	0.6	0.75	0.9	1.05	1.2	1.35	1.5
Measured magnet strength (T)	0	0.16	0.30	0.46	0.60	0.76	0.91	1.05	1.21	1.35	1.47

As it was possible that the Bruker magnet was having a small effect on the magnetic field in the surrounding rooms, the performance of the nearby clinical linacs (U5 and U7) was checked. Linac error plots with the magnet on and with the magnet off were made. The steering servo's were off. A servo is a control mechanism of the linac. The steering servo adapts the 2R and 2T currents based on the measurements of the ionization chamber, to get the measured symmetry back to zero. The servos must be switched off in order to observe the influence of an external system such as the Bruker magnet.

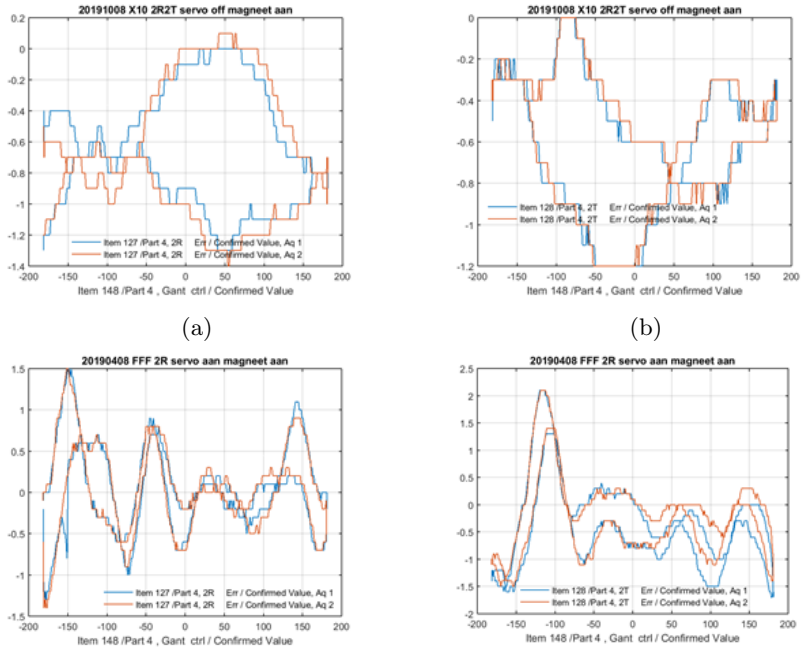

Figure 7: The 2T and 2R linac symmetry error plots of U5 and U7 with the Bruker magnet turned on (blue) and off (red) at U4. The horizontal axis shows the gantry angle, the vertical axis the linac symmetry error. The plots show no difference between magnet on and magnet off.

As can be seen from figure 7, there was no clear difference between magnet on and magnet off. From this experiment it was concluded that it is safe to use the magnet when the U5 and U7 are in use.

When the Bruker magnet was on, the linac U4 was affected by the additional stray magnetic field. Inline and crossline profiles were measured with a starcheck attached to the head of the linac at gantry 84 degrees for every available magnetic field strength. If there was an influence of the magnetic field, the position of the field would change with magnetic field. The center of the field and position of the beam peak of the FFF field were analyzed. The results were shown in figure 8. The starcheck was not aligned exactly in 0,0, so the absolute error value gives no information. It could only be used to see the change in position.

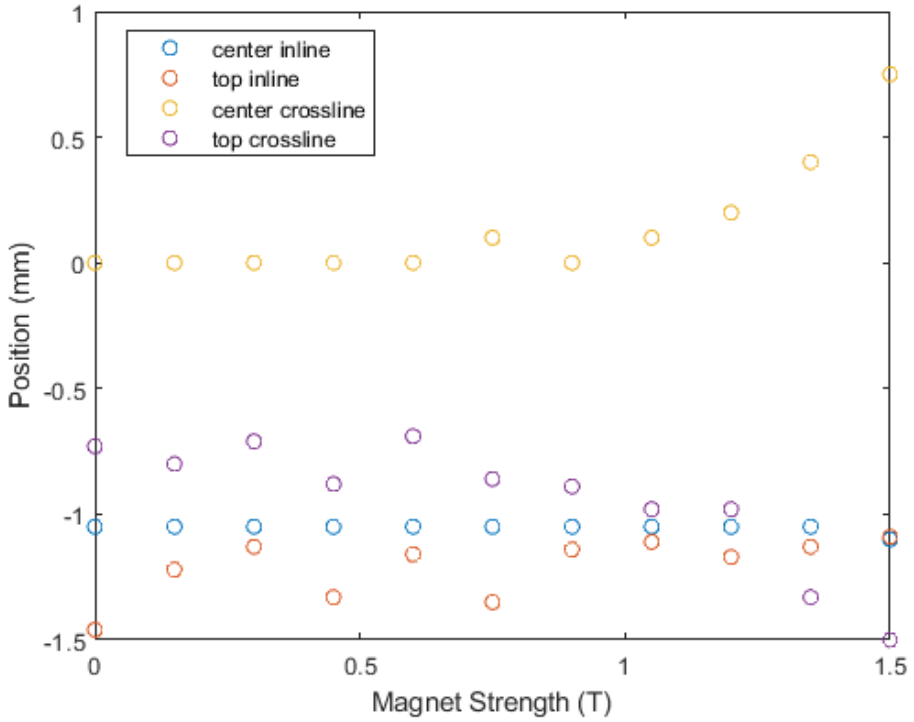

Figure 8: Results of the Starcheck measurements of field centre and beam peak for both inline and crossline directions. Crossline 2T servo was off. A variation is seen for crossline center and beam peak at high field strength.

It can be seen that mainly in the crossline direction, the magnet influenced the position of the beam peak and the center of the field. This influence was smaller in the inline position. This would be explained by the servo which is on in the inline direction, but off in the crossline direction. This is the same as for our clinical machines, for which it is not allowed by the vendor to turn on the servo in the crossline direction for FFF. To see if turning the servo on would decrease the field strength dependency, the same measurements were repeated with the 2T servo on. The results are shown in figure 9.

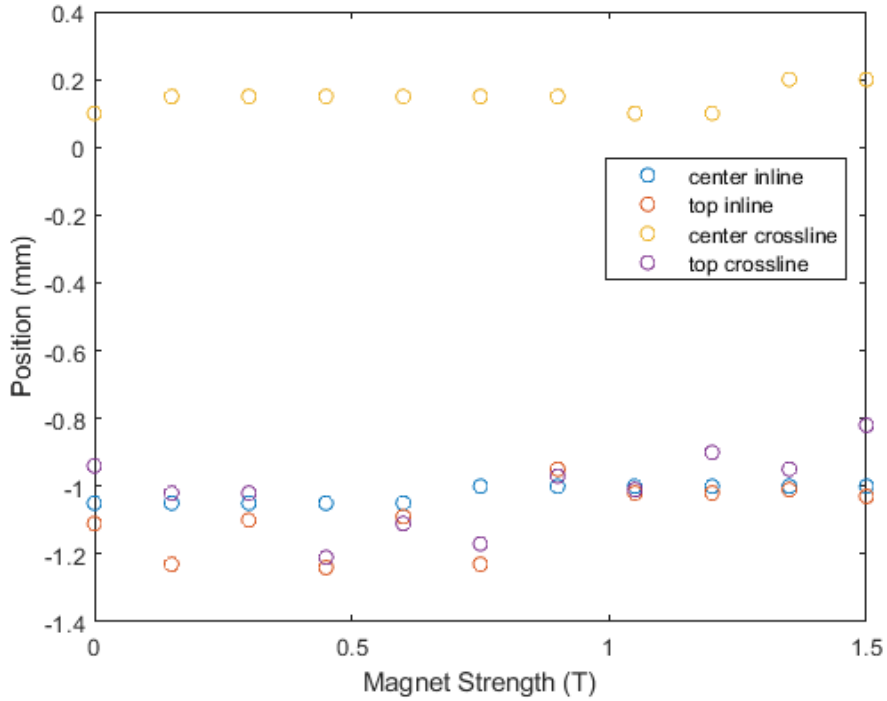

Figure 9: Results of the Starcheck measurements of field centre and beam peak for both inline and crossline directions. Crossline 2T servo was off. No variation is seen anymore for crossline center and beam peak at high field strength.

As can be seen in figure 9, with the 2R and 2T servos switched on, the change in magnetic field does not affect the beam. The 2T servo will be on for the experiment. These preparatory steps and measurements established that the linac, the beam and the magnet are suitable for the experiment.

4.3 Methods and materials

For the first experiment 26 gel vials were used, all from the same batch. The gels were irradiated with the 6 MV Flattening Filter Free (FFF) beam of the U4 with a 3x3 cm^2 field at the Bruker magnet. The magnetic field was introduced by the Bruker magnet. To create the 3x3 cm^2 field between the pole shoes, a tertiary collimator was used, combined with a 5x5 cm^2 field (at isocenter) of the linac formed by the leaves and jaws. This tertiary collimator was placed at the table. As a reference, an ionization chamber was placed in front of the tertiary collimator. The gantry was at a angle of 84 degrees. The vials were placed in a rectangular water phantom with 5 cm of water in front of and behind the vial. The phantom was placed between the pole shoes of the Bruker magnet. The setup is shown in figure 10. Dose-rate was kept the same for all vials. The vials were all stored together in a water bath, so that the temperature was as constant as possible and they all experienced the same environment.

(a) (b) (c)

Figure 10: Setup of the experiment: (a) Vial placed in phantom, between pole shoes (b) View from the linac, tertiary collimator on table with reference ionization chamber in front (c) Total overview of setup

The 26 vials were all irradiated using a different combination of dose and field strength. Doses of 1, 2, 4 and 8 Gy were irradiated in magnetic fields strengths of 0.00, 0.15, 0.30, 0.60, 1.05 and 1.45 T. Field strengths were measured before the irradiation of each vial. One vial was kept at 0 Gy, and one vial was irradiated up to 4 Gy at gantry 0 degrees in a water tank with a 10x10 cm^2 field at depth 10 cm as control (field strength 0 T). To determine the amount of monitor units (MU) needed to give a certain dose, dose measurements were done at 0 T and 1.5 T before starting the experiment between the pole shoes of the Bruker. Dose measurements were done with an ionization chamber in the same phantom as used for the experiment. The ionization chamber was placed at the same place as the gels later. The measurement at 1.5 T was corrected with a k_B factor. The 0 T value was used to calculate the amount of MU needed. The difference was within 1%. Since this difference was within 1%, it was not corrected for in the amount of MU. The difference in dose was used to correct the measured dose later. All vials were irradiated consecutively on the same day.

After irradiation, the vials were scanned at a 1.5 T Philips Ingenia MRI scanner. Scans were made after 1, 2, 4 and 8 days. To do T2 mapping a 3D Carr-Purcell-Meiboom-Gill (CPMG) sequence with 32 echos was used (FOV 148x148x62 mm^3, resolution 2x2x4 mm^3, TSE, TE 40 ms, TR 2000 ms, total scan durating 41:06 mm:ss). The vials were also scanned with a 2D sequence with 20 echoes (FOV 144x144x130 mm^3, resolution 2x2 mm^2, slice thickness 2 mm, TSE, TE 40 ms, TR 2000 ms, total scan duration 12:06 mm:ss). For the analysis, a volume of interest (VOI) was created in the irradiated area of each vial. The volume of this VOI was about 2 ml and had a margin of about 4 mm from the edges of the vial and the bottom of the irradiated part. For this VOI, the average signal intensity was determined for each echo. By fitting this curve, the T2 value was determined. The fit was done using a single term exponential fit, using the Matlab fit 'Exp1'. The first echo was discarded [56]. The mathematical form of the fit is shown in equation 10.

$$S_i = M_0 * exp^{-TE_i/T2} \tag{10}$$

The R2 value is defined as 1/T2.

4.4 Results

4.4.1 Linearity

The R2 results for the different CPMG scans are shown in figure 11. As can be seen from the figure, the R2 is proportional to dose for all magnetic field strengths. The average correlation coefficient R^2 is 0.9970.

As expected, there is a change in R2 over time [11]. This change can be seen in figure 12. The linearity does not change, with average R^2s of 0.9972, 0.9969 and 0.9966 for day 2, 4 and 8. The dose measurements at 1.5 T were used to correct for the dose. The 2D scans show similar results.

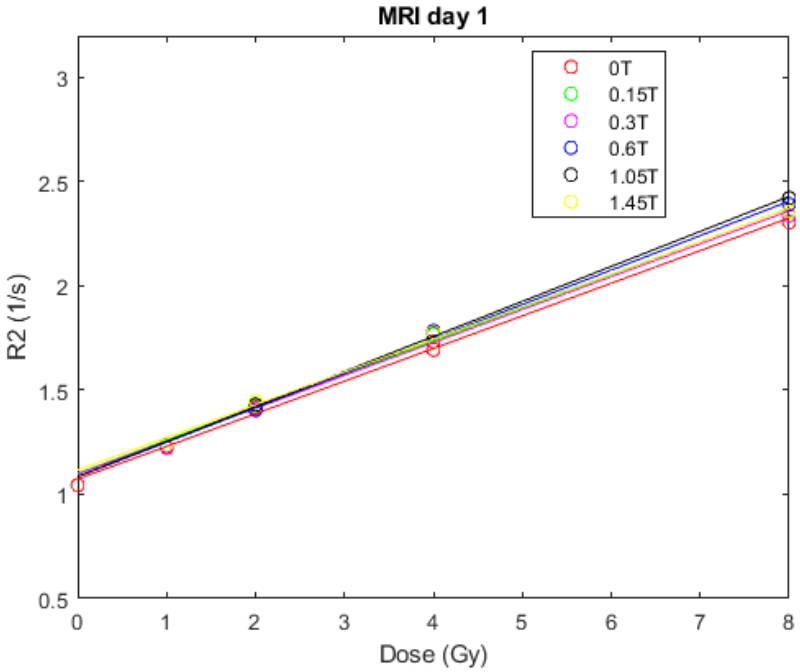

Figure 11: R2 vs dose plots for the scan made 1 day after irradiation. R2 versus dose is linear for all magnetic field strengths.

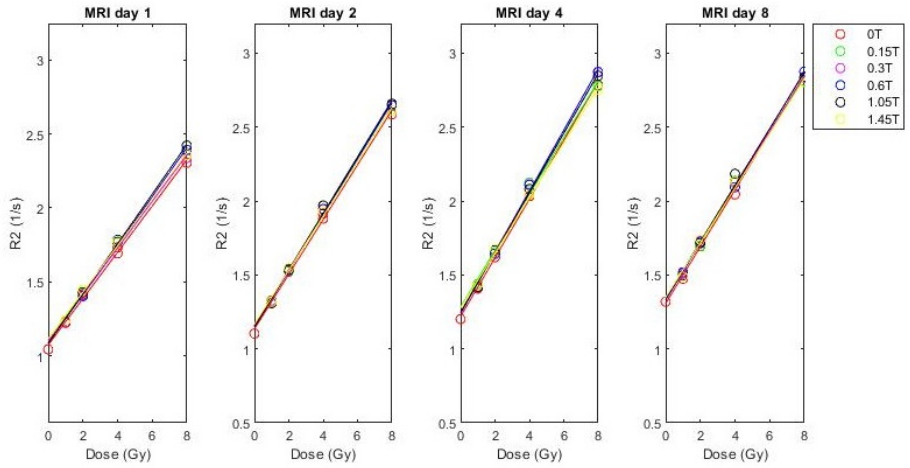

Figure 12: R2 vs dose plots for the scans made during days 1, 2, 4 and 8 after irradiation. R2 versus dose stays linear over time, but the fit offset and gradient change.

4.4.2 Magnetic field dependency

To see if the results are magnetic field strength dependent, the R2 was plotted against the magnetic field strength. This is shown in figure 13. As can be seen, the results are equal for all magnetic field strengths. Average slope of the fit through all values for one dose was 0.0095 with a standard deviation of 0.018. The results were also normalized by dividing the R2 values by the 0 T R2 values for the same dose. These results are shown in figure 14. Small variations in the data were seen, but there is no trend with magnetic field strength.

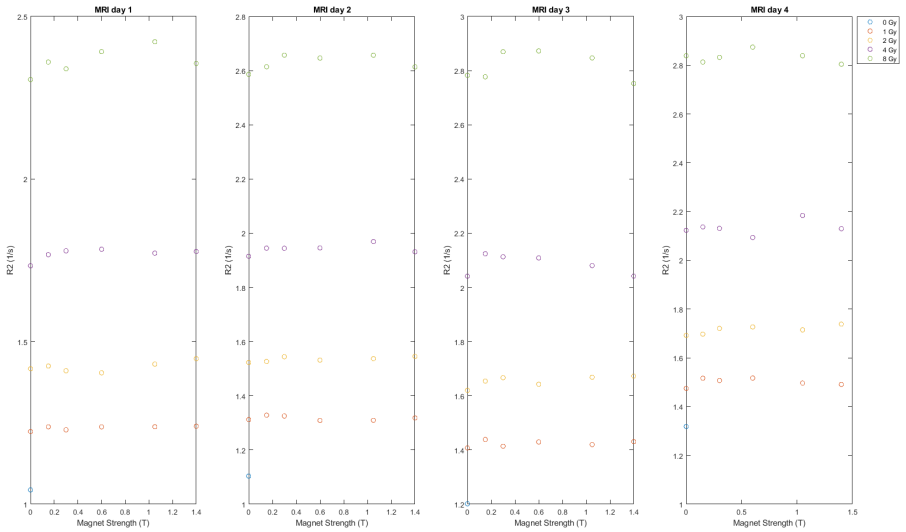

Figure 13: R2 vs magnetic field strength plots for the scans made during days 1, 2, 4 and 8 after irradiation. There is no trend seen in R2 versus magnetic field strength.

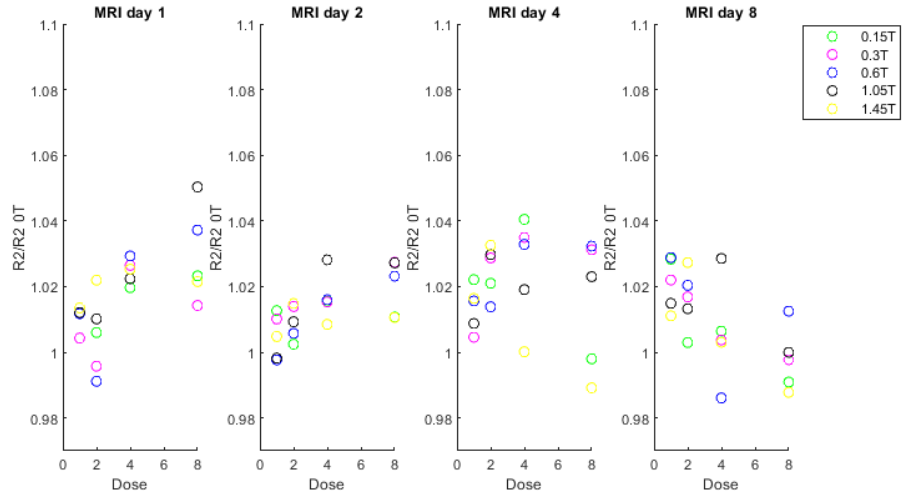

Figure 14: The R2 for each dose and magnetic field strength divided by the R2 of the corresponding dose at 0T. There is no trend with field strength.

The vial irradiated under reference conditions was used to determine the R2 for a dose of 4 Gy. The value was 9.6% higher than the equivalent R2 value measured in the Bruker magnet. If this control was used to calculate the dose in the other vials, 1, 2, 4 and 8 Gy would be approximately 0.91, 1.82, 3.65 and

7.3 Gy. This is quite a large difference, probably caused by the uncertainties in the dose measurement between the pole shoes due to, for example, magnetic field correction factor and distance. This did not influence the results of the experiment, it is only a scaling factor. It does not influence the R2 linearity or magnetic field dependence.

4.5 Discussion

The results in the linearity section show that R2 is linear with dose for magnetic fields up to 1.47 T and doses between 1 to 8 Gy. It was also shown that the R2 versus dose stays linear over time, only the offset and slope of the fit changed. This is caused by polymerization and gelation processes after irradiation. The assumption is that if the gel behaves the same for doses from 1 to 8 Gy, it will also behave the same for doses below 1 Gy or above 8 Gy, but this was not proven in this experiment. It is assumed that the gels also stay linear up to 42 Gy in magnetic fields, consistent with previous results that show the R2 versus dose stays linear up to 42 Gy without magnetic field. If R2 versus dose is linear, the gels can be used for relative dosimetry, and with some additional calibration also for absolute dosimetry. There are no publications for doses below 2 Gy. In this experiment, the lowest dose was 1 Gy, therefore the accuracy of dosimetry for doses lower than 1 Gy has not been validated. In clinical treatment plans, if doses of less than 1 Gy are relevant to organs at risk or normal tissues, than the accuracy of these doses can be verified by further experiments. It is only needed to test this for one magnet strength, since the behavior for other magnetic field strengths is consistent.

The results in the magnetic field dependency section show that there is no significant effect of the magnetic field. If the R2 for each dose and magnetic field strength is normalized by the R2 of that same dose for 0 T, no trend with magnetic field is observed. Noise can be seen in the normalized values. The experiment could be improved by making multiple scans on the same time point, so that the T2 can be determined more exactly. It would also be an option to irradiate more vials, so that for every combination of dose and field strength 2 or 3 T2 values could be averaged. The magnetic field independence was only verified for magnetic field strengths up to 1.47 T. Higher field strengths were not investigated, however no field strength dependence was seen and therefore none is expected for higher magnetic field strengths.

The MR sequence was provided by the vendor and not further optimized. It might be possible to optimize the MR sequence to get a higher SNR, sensitivity and/or shorter scanning times. That was not within the scope of this project.

4.6 Conclusions

The first hypothesis of this experiment was that the gel relaxation rate R2 was linear with dose in magnetic fields. This was confirmed for magnetic fields between 0 T and 1.47 T and doses of 1 to 8 Gy.

The second hypothesis of this experiment was that the gel response was independent of magnetic field strength. This was confirmed, all responses were consistent. This makes the use of VIPAR gels for dosimetry in MR linacs possible.

5 Experiment 2 - Time dependency of VIPAR gels

5.1 Goal and outline of experiment

To perform an end-to-end test including positional accuracy, it is desirable to read-out the vials at the same place as they were irradiated. Therefore, read-out within approximately one hour should is desirable. No results have been published for VIPAR gels for scanning within 24 hours. Previous research showed that the time between irradiation and MR scanning changes the R2 values. The R2 values increase in a time period of 40 days, but the R2-dose response stays linear. For a conventional linac, optimal time between irradiation and scanning is one day to three weeks [35]. Research question 2 is how does the VIPAR gel behave over time after irradiation? The question is divided in three subquestions: 1) What is the trend over time or variation of the gel and is it possible to model this? 2) When would be the best moment to scan the gel? Would it be possible to scan the gel within one hour after irradiation? 3) Is it possible to scan and irradiate at the same time, how precise can the dose be determined?

The experiment was conducted at a 1.5 T Elekta Unity MR-linac (Elekta, Stockholm, Sweden). Three vials were irradiated to doses of 4, 8 and 12 Gy. MR sans were made during the irradiation, immediately after irradiation, and continuing until 3 days after irradiation, all without moving the phantom. Additional scans were made after 1, 2, 3 and 4 weeks by putting the phantom back in the MR-linac. To be able to see differences in the gel on short time differences, the MR sequence should be as short as possible. The sequences used in the first experiment were respectively 43 and 12 minutes for the 3D and 2D sequence. In the preparation section adaptations to the MR sequences to make them faster are discussed. Sections 5.3, 5.4, 5.5 and 5.6 describe the methods and materials, results, discussion and conclusions of the experiment.

5.2 Preparation

5.2.1 Preparation for the MR

To see the differences in the gel during or shortly after irradiation, it is important to have a MR sequence that is as short as possible. The scans from the first experiment took 41 minutes for the 3D sequence with 32 echoes and 12 minutes for the 2D sequence with 20 echoes. This is too long for scanning during or immediately after irradiation. First, an analysis of the data from the first experiment was done to see if less echoes could be used while maintaining accuracy. The T2 was fitted with different numbers of echoes as input data. The calculated T2 values were then compared with the T2 values of the original scan. This was done for the 3D CPMG sequence as well as for the shorter 2D sequence with 20 echos. The results of this analysis are shown in figure 15. The results shown are from the scan after 48 hours. The other scans show similar results. This analysis shows that for both sequences, at least 17 echos are needed to limit the error to within 1%. Another way to reduce scan time would be to reduce the number of slices acquired. This was tested with a diagnostic 1.5 T MRI by scanning the same 26 vials with different combinations of slices and echos. This was done for the 3D CPMG sequence as well as for the 2D

sequence. The combinations scanned are shown in tables 2 and 3.

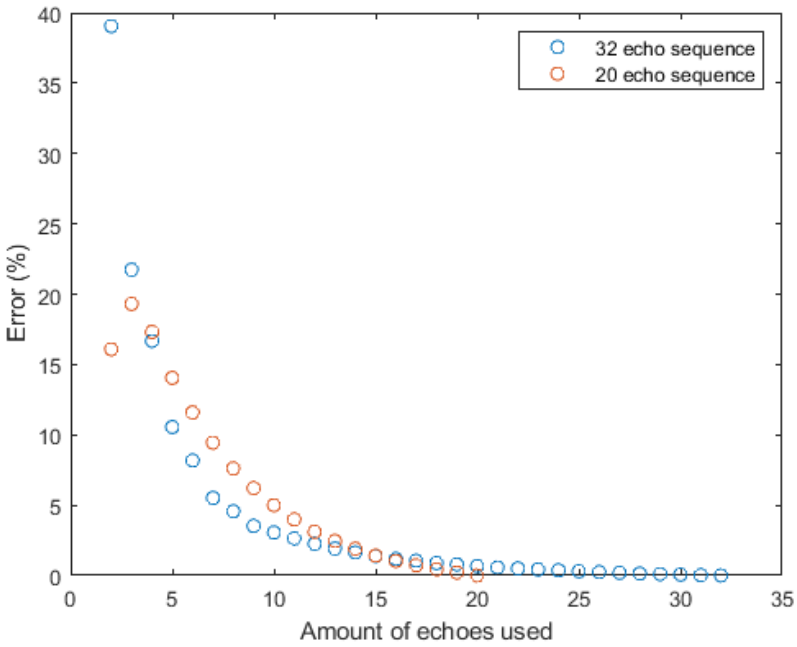

Figure 15: Difference in T2 determination when using less echoes than the full 20 or 32 echo sequences. At least 17 echoes are required to achieve an accuracy within 1%.

Table 2: The combinations of number of slices and echos scanned for the 3D CPMG sequence.

Slices\echos	32	16	8
31	✓	✓	✓
15	✓	✓	✓
10	✓	✓	✓
7	✓	✓	✓

Table 3: The combinations of number of slices and echos scanned for the 2D sequence.

Slices\echos	20	16	10	8
65	✓	✓	✓	✓
30	✓	✓	✓	✓
20	✓	✓	✓	✓
15	✓	✓	✓	✓
10	✓	✓	✓	✓

In total 32 scans were made. 12 for the CPMG sequence and 20 for the 2D sequence. For each scan the T2 was fitted and compared with the T2 of the scans with all echos and slices (31 slices and 32 echos for the CPMG sequence, 65 slices and 20 echos for the 2D sequence). The results of those scans are shown in tables 4 and 5. The difference was calculated by $(T2_{new}/T2_{originalsequence} - 1) * 100\%$. The difference was calculated for each of the 26 vials, from which the mean error and standard deviation were determined.

Table 4: The results for all scan combinations made for the CPMG sequences. A reduction in echoes increases the error, a reduction in slices leads only to a small increase in error.

Slices	Echoes	Time (m)	Mean error (%)	Std (%)
31	32	41.1	0	n.a.
31	16	20.6	3.3	0.88
31	8	10.3	6.2	0.18
15	32	20.6	0.25	0.19
15	16	10.3	3.4	0.90
15	8	5.2	6.2	1.8
10	32	13.2	0.75	0.57
10	16	6.6	3.3	1.0
10	8	3.3	6.7	1.9
7	32	10.3	0.95	5.5
7	16	5.2	3.0	1.2
7	8	2.6	6.4	1.9

Table 5: The results for all scan combinations made for the 2D sequences. A reduction in echoes increases the error, a reduction in slices leads only to a small increase in error.

Slices	Echoes	Time	Mean error (%)	Std (%)
65	20	12.1	0	n.a.
65	16	9.9	1.4	0.66
65	10	4.4	4.6	2.1
65	8	3.67	3.0	1.6
30	20	5.5	0.71	0.40
30	16	4.5	1.5	0.68
30	10	2	4.5	2.2
30	8	1.67	3.0	1.8
20	20	3.67	0.51	0.38
20	16	3	1.7	0.80
20	10	1.4	4.6	2.3
20	8	1.17	2.7	1.7
15	20	2.93	0.63	0.50
15	16	2.4	1.7	0.83
15	10	1	4.4	2.2
15	8	0.83	2.4	1.6
10	20	1.83	0.68	0.52
10	16	1.5	1.4	1.0
10	10	1	3.4	1.9
10	8	0.83	1.7	1.3

From those tables it can be concluded that reducing the amount of slices has less influence on the error than reducing the amount of echos. The 2D scan with 10 slices and 20 echos has an error within 1% and takes 1 minute and 50 seconds.

Since the diagnostic MR is not exactly the same as the MR from the MR-linac, the MRI Examcards had to be adapted to be suitable for the MR-linac. An Examcard contains all information about one or multiple sequences. Based on the results from the previous tests on the diagnostic MRI, new sequences were created on the MR-linac. The sequence that will be mostly used for the experiment is a coronal 20 echoes 2D sequence with 18 slices of 4 mm and a echo time of 20 ms. It takes 1 minute and 12 seconds to execute the sequence. It gives the images of the 20 echoes and a T2 map calculated by the MRI. Next to this sequence, two other sequences were also scanned if more time was available between two consecutive scans to see if there was a difference between sequences. This were a 32 echoes sequence with a echo time of 40 ms and a 3D sagital scan with 16 echoes and an echo time of 25 ms. Those scans took respectively 22 minutes 26 seconds and 5 minutes 6 seconds. The 2D sequence with 20 echoes was tested with three vials from experiment 1. The vials show a linear R2 versus dose response. The 32 echoes sequence shows also linear behavior for the R2 values.

5.2.2 Preparation for the irradiation

The vials in the phantom have to be irradiated with doses of 4, 8 and 12 Gy. To do this, the phantom was scanned with a CT and a dose calculation was made with the Monaco planning system. A screenshot of the plan is shown in figure 16, the cumulative dose volume histograms (DVHs) are shown in figure 17. The dose was given in 6 segments. Three segments were delivered from gantry 90 degrees and three segments from gantry 270 degrees. The first segment for both gantry angles consisted of a large field, which gave 2 Gy to all the vials. For the second segment, the field size was decreased to cover only two vials and delivered another 2 Gy. The third segment gave another 2 Gy to only the last vial.

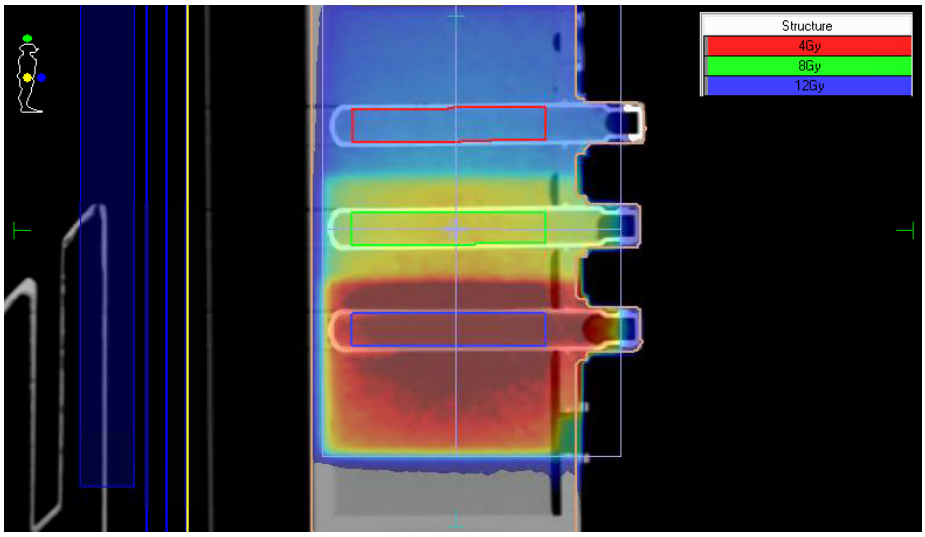

Figure 16: Screenshot of the plan in the TPS. The red line indicates the area which should receive 4 Gy, the green line area is the area that should receive 8 Gy, and the blue line is the area that should receive 12 Gy.

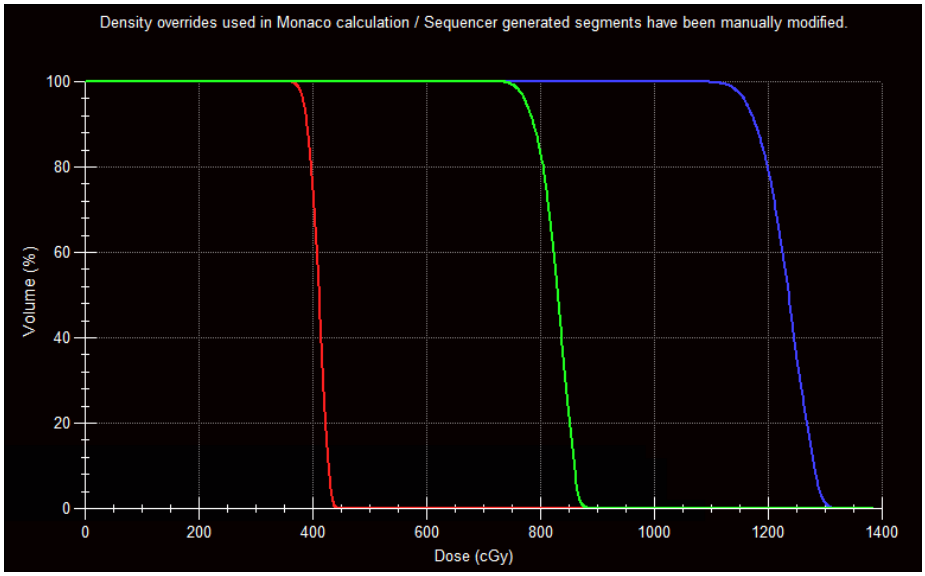

Figure 17: Screenshot of the DVH's in the TPS. The red DVH is the DVH of the volume that should receive 4 Gy, the green DVH is the DVH for the volume that should receive 8 Gy, the blue DVH is the DVH for the volume that should receive 12 Gy.

To test if the dose inside the vials was really 4, 8 and 12 Gy, gafchromic film was placed inside water-filled glass vials and the plan was executed on the films. The film was analyzed using in-house developed software (GirafTool). This gave the results shown in figure 18. The absolute dose read-out was higher than expected, but there was no calibration film, the dose was calculated with an existing OD to dose curve. Thus the absolute doses calculated were only an approximation, but the relative dosimetry, the ratio of doses, could still be accurately determined. The ratio between the three lines was corresponding with the ratio of 4, 8 and 12 Gy.

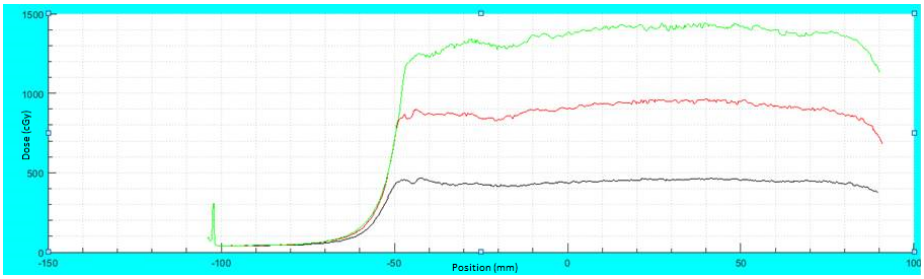

Figure 18: Profiles of the measured doses on the films used to check the plan. Expected doses are 4, 8 and 12 Gy. All doses are higher than expected. The films were not calibrated for accurate absolute dose measurements, however, the ratio of doses could be determined and is corresponding to the ratio of 4, 8 and 12 Gy. The low dose that is seen between position -100 and -50 is the unirradiated top of the film.

5.3 Methods and materials

Three gel vials were used for the experiment. A overview of this setup is shown in figure 19. During irradiation, 4.8 cm of buildup slabs was placed to the sides of the phantom. Those slabs were removed after irradiation, so that the coil could be lowered for a better SNR. The phantom was aligned to the lasers, which are mounted to the walls. The phantom with the irradiated vials is shown in figure 20.

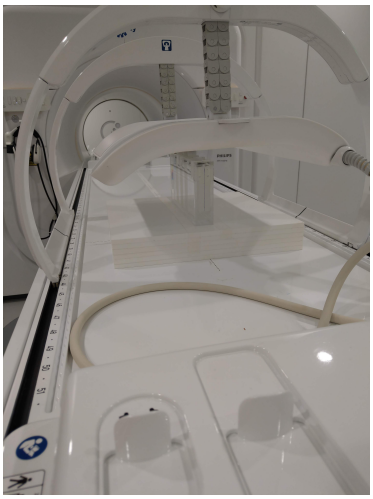

Figure 19: Placement of the phantom and the coil, shown outside the bore.

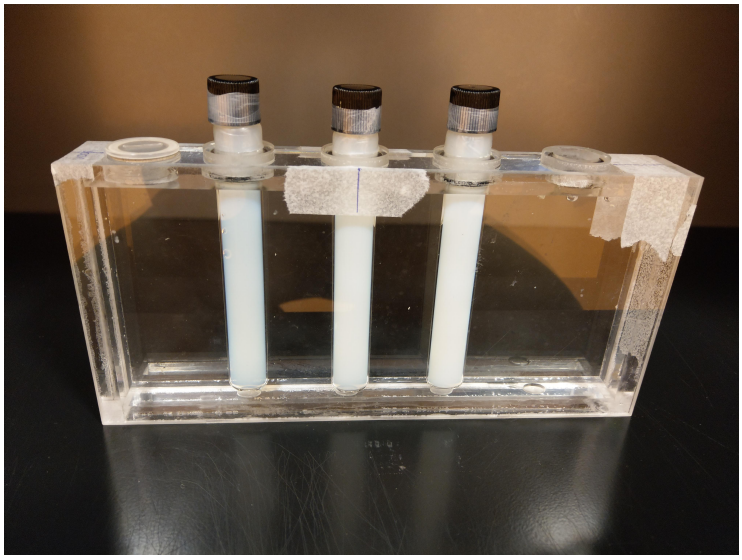

Figure 20: Phantom and gel vials used to test VIPAR gel time dependency. Vials have already been irradiated.

Three different sequences were used to scan the phantom. The most used sequence was the 20 echo sequence (FOV 150x47x80.5 mm^3, resolution 2x2 mm^2, slice thickness 4 mm, TSE, 20 echoes, TE 20 ms, TR 2000 ms, total scan duration 1:12). The other two sequences were the 16 echo sequence (FOV 150x128.6x40 mm^3, resolution 2x2x4 mm^2, TSE, 16 echoes, TE 25 ms, TR 2000 ms, total scan duration 5:06) and the 32 echo sequence (FOV 150x37.5x80 mm^3, resolution 2x2x4 mm^3, TSE, 32 echoes, TE 40 ms, TR 2000 ms, total scan duration 22:50). The experiment was performed on Friday the 6th of March 2020, starting at 14.00. Four 20 echo scans were made during irradiation. After

irradiation, the buildup slabs were removed and the coil was lowered. The first 20 echo scan after irradiation was then made after 4 minutes. After this, scans were continuously made until 30 minutes after the irradiation. From then on the time interval between scans was ascending and also the longer 16 and 32 echoes sequences were scanned. Scans were made until monday morning 7.00 with the phantom in exactly the same position. For the scans afterwards, the phantom was removed and placed back for each scan. For those scans, the phantom could have been in a slightly different position. Therefore, new VOI's were drawn if the position was different. Scans were made until 43 days after irradiation.

For the analysis, a VOI of about 6 ml was created at the homogenously irradiated area of the vial. For this VOI, the mean signal intensity was determined. The T2 was fitted using the signal intensities from all echoes, the first echo was discarded [56]. Equation 10 was used.

5.4 Results

5.4.1 Time dependency of gel

In total, 57 scans at different timepoints were made with the 20 echo sequence. The results of those scans are shown in figure 21. The first scan was made at the start of the irradiation, the last scan was made after 43 days.

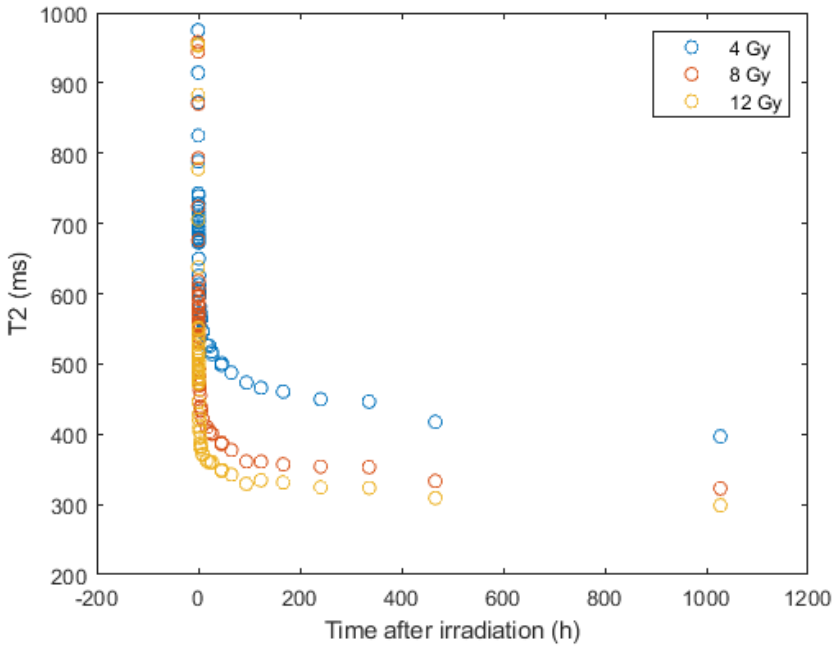

Figure 21: The T2 values for the three vials of 4, 8 and 12 Gy for all scans made with the short 20 echo sequence.

For this sequence, the software of the MR also creates a T2 map. The comparison of the results from the MR software and the results of the self-written matlab fit are shown in figure 22 and 23. These figures show that the obtained T2 values are almost identical. The largest error was 6.4 ms on a T2 time of 674 ms, less then 1%. This indicates that the code written in matlab is able to fit the right T2 value and so can also be used for sequences where the MR does not give a T2 map.

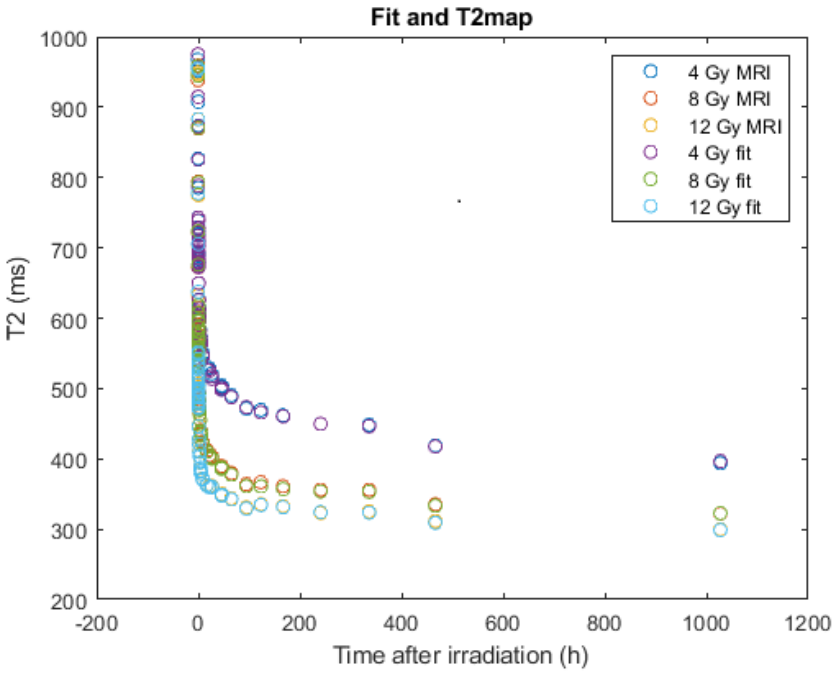

Figure 22: The fitted T2 values for the three vials of 4, 8 and 12 Gy for all scans made with the 20 echo short sequence in comparison with the T2 values calculated by the MR software.

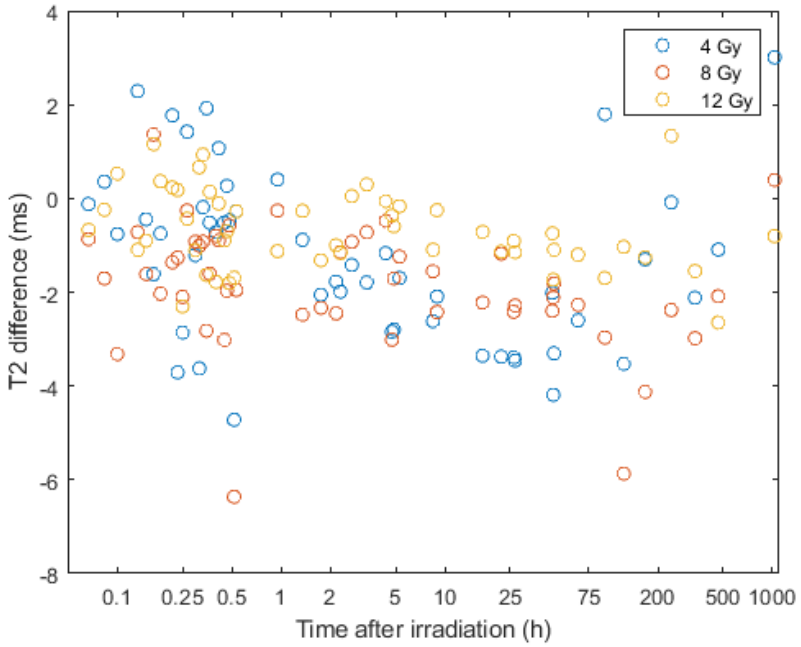

Figure 23: Visual representation of the relative difference between the matlab T2 value and the T2 value of the Philips software. Time is plotted on a log scale. The difference is calculated by $T2_{matlabfit} - T2_{Philips}$. Largest difference seen was 6.4 ms, which was less then 1%.

The other sequences with 32 echoes and 16 echoes were scanned respectively 21 and 17 times. The comparison of the results from the different sequences is shown in figure 24. The different sequences show the same behavior of the gel, but with (slightly) different T2 values. Since we are mostly interested in the data shortly after irradiation and for this, the short 2D sequence with 20 echoes has the most data points, most of the analyses hereafter will be on the data from this sequence. The other sequences were acquired to see if there is a difference between sequences.

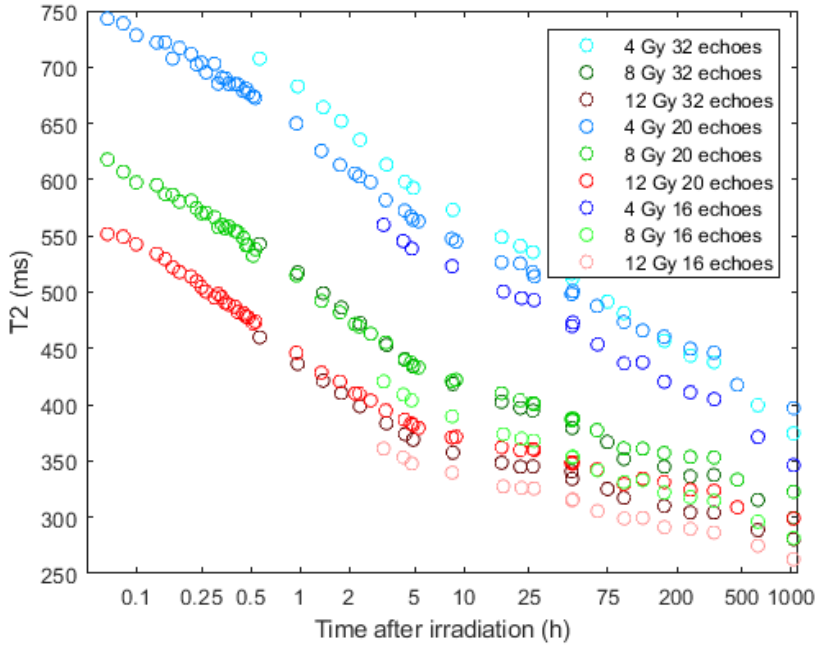

Figure 24: T2 values for the three vials of 4, 8 and 12 Gy for all scans made with the three different sequences. The curves show comparable behavior for the different sequences, but different T2 values. Demonstrating that for comparisons between multiple measurements, or for absolute dosimetry, the same sequence must be consistently used.

5.4.2 Fitting the plots

After plotting the results, the question was whether it was possible to make a fit through all data points for one dose. The first four scans were not used for the fit, because there the full dose had not yet been delivered. The first attempt was to fit the point with a simple logaritmic fit which looks like y=a+b*ln(x). If the data points would follow this curve exactly, this would also mean that if you plot the data on a log-time scale, the plot would be linear. This is shown in figure 25. As can be seen from figure 25, a linear fit through this data is clearly not optimal. As was also described in the introduction, the time stability of the gel depends on two processes, the polymerization of the monomers and the gelation of the gelatin. The polymerization of the monomers is a shorter process, supposedly up to 12 hours. The gelation process takes longer. From figure 25 it can be seen that for this VIPAR gel, the turning point seems to be around 7 hours instead of 12 hours.

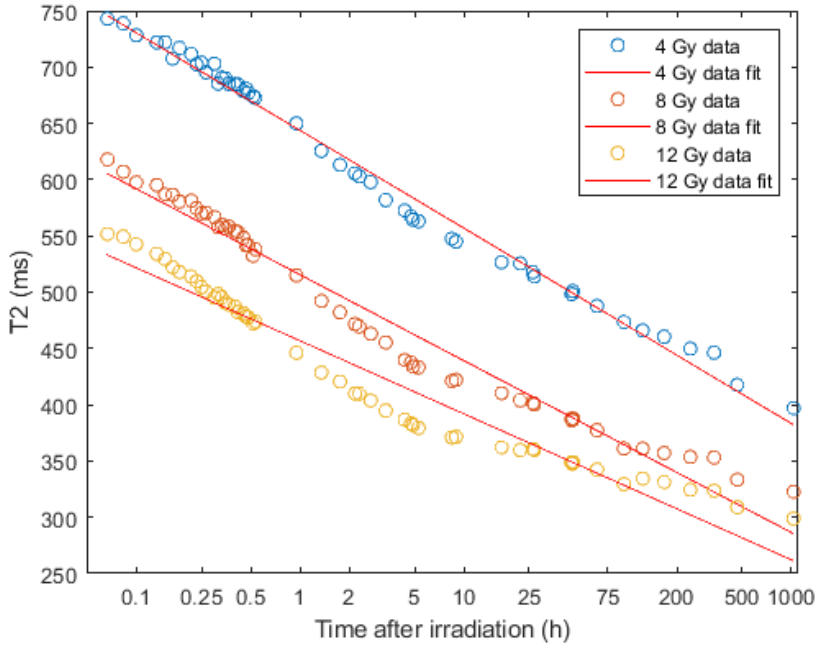

Figure 25: Linear fit through the data points for each dose, when the time is plotted on a log scale. The linear fit does not give a good description of all data points.

Given those two processes, it makes sense to split the fit up into two parts. The first part for the behavior including the polymerization process, the second part for where only the gelation plays a role. The results for those fits are shown in figure 26. Mean R^2 for all fits during the first 7 hours is 0.9958, mean R^2 for the fits after 7 hours is 0.9828. The linear fits can be described by $y = ax + b$, with y the T2 value, and x the natural logaritm of the time in hours. The values for a and b are shown in table 6.

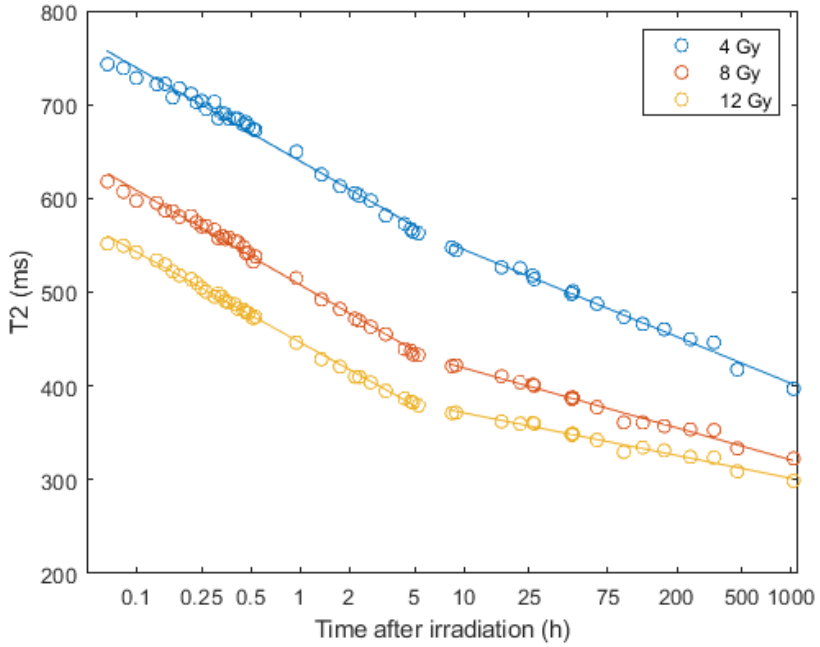

Figure 26: All data points for the 20 echo sequence with 2 linear fits for each dose. The first linear fit for data points before 7 hours, the second linear fit for data points after 7 hours.

Table 6: The values for a and b of the linear fits

Dose	a (up to 7 hours)	b (up to 7 hours)	a (after 7 hours)	b (after 7 hours)
4 Gy	-0.0489	0.6451	-0.0311	0.6171
8 Gy	-0.0494	0.5133	-0.0213	0.4684
12 Gy	-0.0471	0.4517	-0.0152	0.4063

Difference calculation With those fits, for each point in time the value calculated by the fit was compared with the measured value. The difference was calculated according to formula 11.

$$Difference(\%) = \frac{Measured\,T2\ from\ data - T2\ from\ fit}{Measured\,T2\ from\ data} * 100 \qquad (11)$$

With this formula, the difference for each dose in each scan was calculated. The results from this are shown in figure 27. As can be seen in this figure, for most scans the difference between the fit and the measured T2 is between -1.5% and +1.5%.

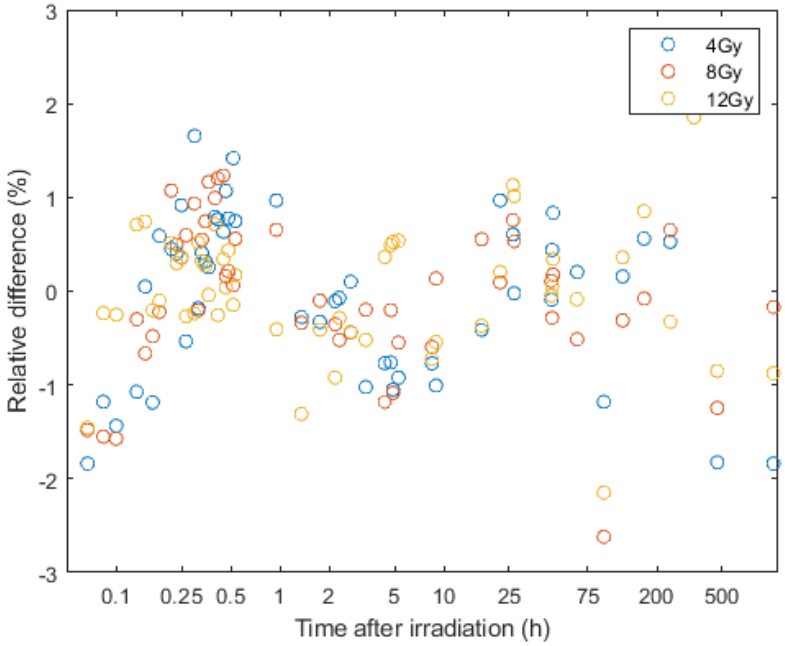

Figure 27: Calculated difference for each scan if the measured T2 value is compared with the corresponding T2 value from the fit. The difference is between -1.5% and +1.5% for most of the scans and seems to become slightly worse after 75 hours.

Difference calculation for the first 4 scans The first four scans were made during irradiation, therefore the dose was increasing while scanning. To be able to calculate the dose in each vial during a scan, the duration of all segments was timed. In combination with the time stamps of the MR scans, it was possible to calculate the dose approximately. There were probably a few seconds between the start of the first MR sequence and the start of the irradiation. This can lead to differences in calculated doses of up to 0.5 Gy. For each vial, the calculated dose was the average of the calculated dose at the start of the scan and the calculated dose at the end of the scan. With the fits from figure 26 and table 6, an expected T2 value for those doses can be calculated. Those expected T2 values are compared with the measured T2 values. The error is calculated again with formula 11. The results are shown in figure 28. The figure shows that for the first four scans, the errors are larger than for the scans made after the irradiation was completely done, but the uncertainty in the calculation is also bigger, because the expected dose is not exactly known.

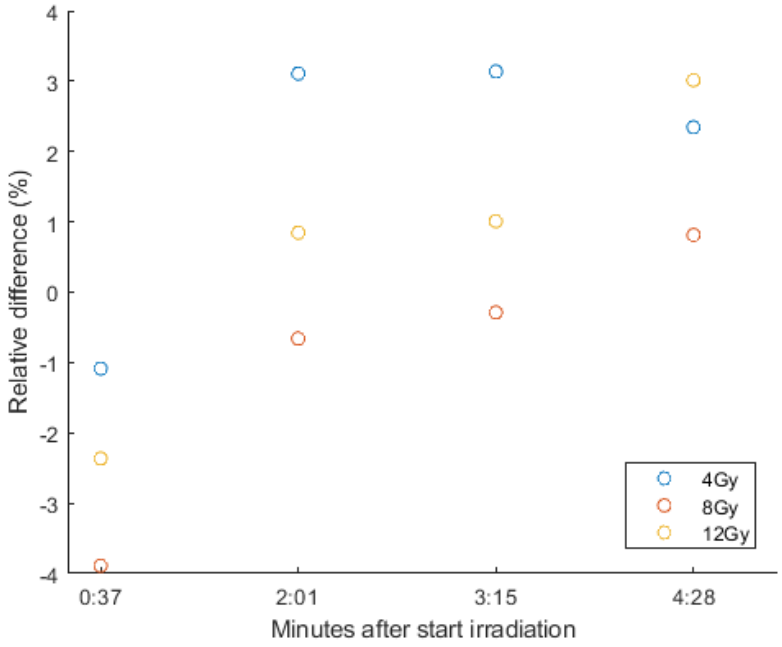

Figure 28: Calculated difference for the first four scans made during irradiation. The expected dose at each scan was calculated and compared with the expected T2 for that dose. Differences are between -4% and +4%.

5.4.3 Change in sensitivity and offset

One of the sub-research questions was what would be the optimal time to scan the gels. To get an answer to this question, the change in sensitivity was analyzed. The sensitivity is the slope of the R2 versus dose graph. In other words, if the R2 is modelled by $R2 = dose * a + b$, a is the sensitivity and b is the offset. The results for the sensitivity and offset over time are shown in figures 29 and 30. It can be seen that the sensitivity reaches a maximum around 7 hours after irradiation and stays quite stable afterwards. The offset b keeps increasing.

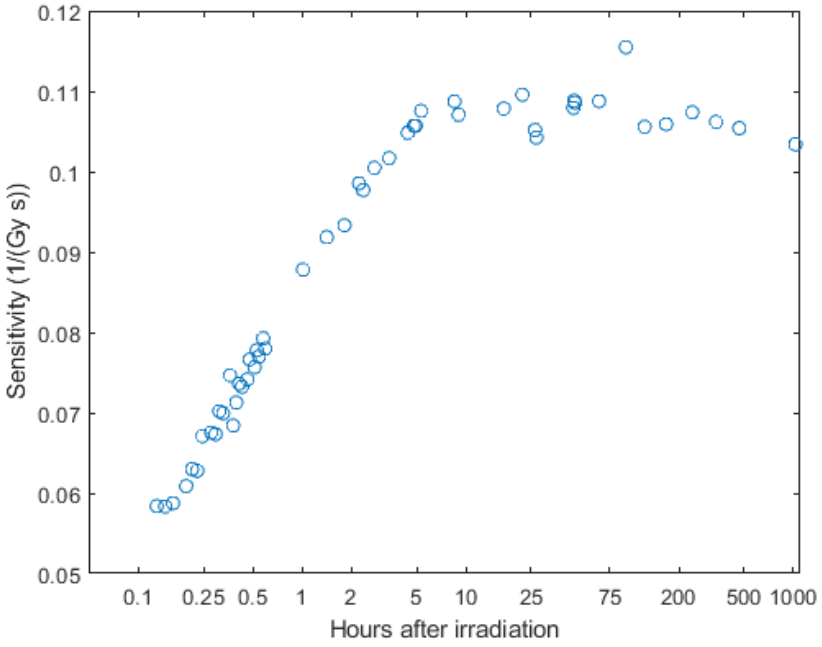

Figure 29: Sensitivity over time. The sensitivity was calculated by determination of the slope of the R2 versus dose curve for each time point. Sensitivity increases up to 7 hours after irradiation and then declines a little bit and becomes stable.

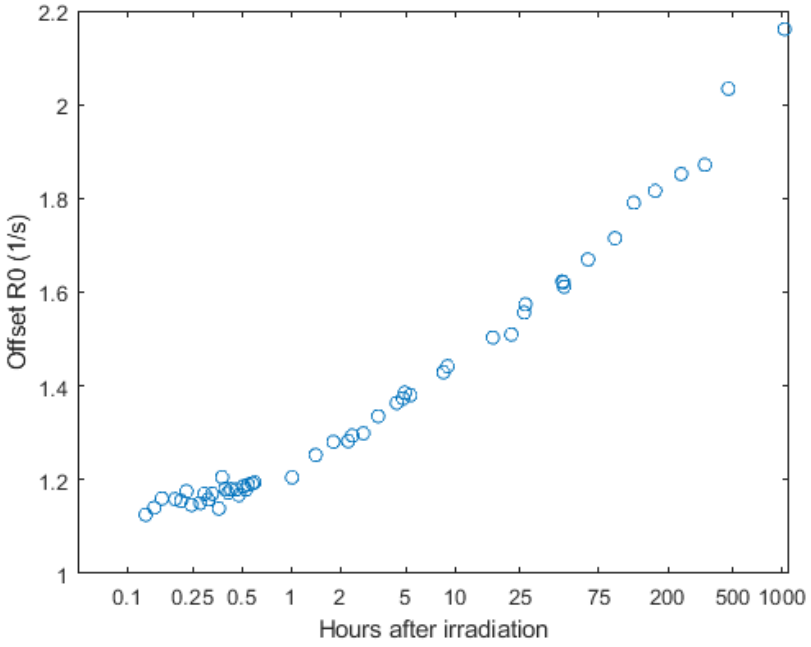

Figure 30: Offset over time. The offset was calculated by determination of the offset of the R2 versus dose curve for each time point. The offset keeps increasing in time.

To see if the linearity changed over time, the R^2 was calculated for the linear fit of R2 versus dose for all time points. The results are shown in figure 31. In this figure it can be seen that the linearity is at its maximum around 20 minutes-1 hour after irradiation. Sensitivity, offset and linearity are all calculated from only three points (4, 8 and 12 Gy), and are thus only approximate values.

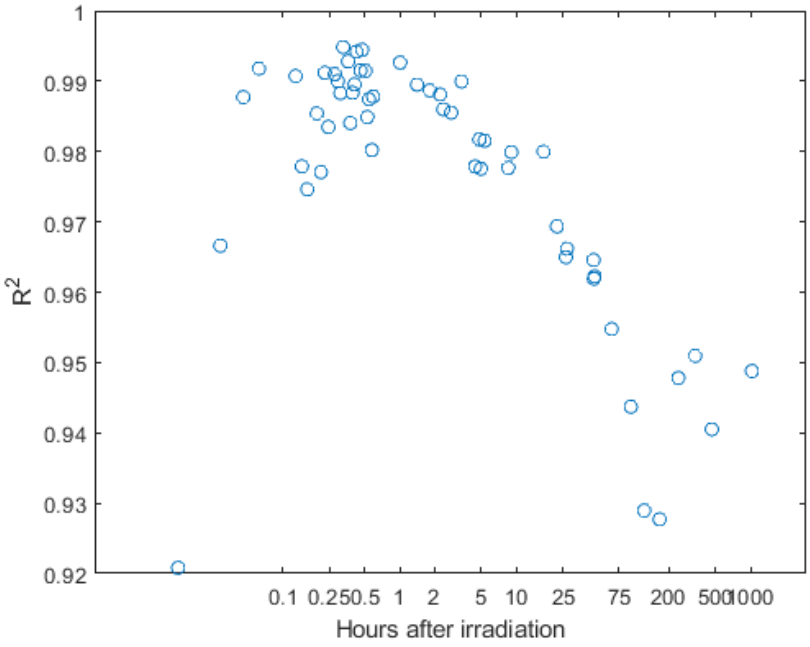

Figure 31: The R^2 for the linear fit of R2 versus dose over time. The linearity declines after approximately 1 hour.

5.5 Discussion

The section 'Time dependency of gel' showed all data points for all moments in time for the different sequences. The sequences showed similar behavior, but do not give exactly the same T2. To see which sequence gives the most realistic T2 value, more research would be required, for example by scanning items with a known T2 value with all sequences. The fit done with matlab was also compared to the T2 value of the MR software. This showed good correspondance.

The section 'Fitting the plots' showed different fits for the data points. The best fits were shown in figure 26. Those fits showed that the fits are also dose dependent. As the R2 was found to be proportional to dose, a calibration curve can be made that is valid for a range of doses. At least in the range of 4-12 Gy as measured here, and probably for a greater range consistent with previous findings with VIPAR gels [13]. Figure 24 also showed that the curves were not exactly the same for the different sequences. This means that an obtained curve can not be used for similar gels of the same batch if a different sequence is used. Also, it should be noted that the fit might be gel-batch dependent. So it is not certain that this data can be used as a calibration for future experiments. Repeating the experiment would be required. What can also be seen in the curves is that the turning point is around 7 hours, instead of the 12 hours indicated in the literature. The difference calculation part shows that most of the points are within -1.5 and +1.5% difference, except for a few outliers. It

also looks like the differences become bigger if the time between irradiation and scanning is larger, starting around 75 hours after irradiation. The differences for the first four scans were also calculated using the fits and the dose linearity. Those differences are 2-3% bigger than the differences when the irradiation was finished. This might partly be explained by the uncertainties in the calculated dose and the time it takes to scan one sequence. Total irradiation time was about 4 and a half minute, in which the sequence was scanned four times. This means that the dose changed a lot between the start and the end of each scan. Ideally, the sequence would be shorter, so that the amount of dose in the gel during one sequence almost does not change and dose delivery should be simultaneous. The R^2 that was determined for the fits of the R2 versus dose for all scans shows an optimum around half an hour after the irradiation. The first two scans show a lower R^2, the third and fourth scan during irradiation show a R^2 comparable to the R^2 after irradiation. The fit is done only on three points, which makes the uncertainty quite large. During the first scan, vial 2 and 3 both had an expected dose of 2 Gy and not exactly the same T2 was measured. This can be caused by noise in the scans or the gels not being exactly the same. This gives problems with the linear fit and explains why the R^2 is lower.

The maximum sensitivity was reached after around 8 hours. This is very different from the optimal sensitivity found by Papoutsaki et al. This could be because they only scanned on days 1, 20, 30, 40 and 50 after irradiation. They do not state after how many hours the scan on day 1 is. If this scan was performed soon after irradiation, it might be that they missed the optimum because they did not have adequate temporal resolution. They also used a slightly different gel, called VIPET, which might have a different maximum. VIPET is a normoxic gel which has tetrakis phosphonium chloride as extra additive compared with VIPAR gel. In agreement is that the sensitivity gets a little bit lower after the maximum and then stabilizes. [35].

5.6 Conclusions

With the results from experiment 2, it is possible to answer research question 2 and its subquestions: How does the gel behave over time? This question is divided in three subquestions:

What is the trend over time or variation for the gel and is it possible to model this? Hypothesis was that it is possible to make a fit, but that it will exist of 2 parts. This was confirmed. The behavior of the gel after irradiation has been characterised, with a 2-part fit, corresponding to the two physical processes - polymerization and gelation. The fits are shown in figures 26 and 27. The difference between the fit and the measured points is for most of the points between -1.5 and +1.5%. This makes it possible to use the curves to predict T2 values or to use the fit to correct for different measurements times. In figure 27, it can also be seen that after 75 hours, the differences seem to become larger. If you want to use the fit to calculate what the T2 value would be at another time point, this might be most accurate for T2 values of scans within 75 hours.

When would be the best moment to scan the gel? Would it be possible to scan the gel within one hour? Hypothesis was that the best moment to scan the gel would be between 1 day and three weeks after irradiation. According to figure 29 this is around 8 hours after irradiation. The sensitivity is then at its

maximum. However, the sensitivity at the beginning is also high enough to be used and the linearity is at maximum after approximately 20 minutes. So the optimal moment to scan depends on what is most important, real-time imaging, sensitivity or linearity. Real-time imaging comes at a cost of sensitivity. Optimal sensitivity is later, but it might not be possible in practice to keep the phantom in place for 8 hours or more. For an end-to-end test where you want to read-out the phantom at the same place as it was during irradiation, read-out should be done after 20 minutes to one hour.

Is it possible to scan and irradiate at the same time, and how precisely can the dose be determined? Hypothesis was that scanning and irradiating at the same time might be possible, but will come at an accuracy cost. Results showed that it is possible to scan and irradiate at the same time. The measurements agreed with the extrapolated fit to within 4%. However, at least some of this difference is due to uncertainty in the predicted dose due to uncertainties in timing. Figure 31 also showed that the linearity of R2 versus dose is at a optimum after about 20 minutes, but that the R^2 for the third and fourth scan (during irradiation) is only slightly less.

6 Experiment 3 - End-to-end test for a MR-linac

6.1 Goal and outline of experiment

To test the complete workflow of a treatment on a MR-linac, an end-to-end test could be performed. The goal of this section is to establish a protocol for end-to-end testing and describe the uncertainties. Generally, an end-to-end test performed at the radiotherapy department of UMC Utrecht uses gafchromic film. Disadvantages of this are that it only gives information in one plane and air gaps around the film can create problems. Using VIPAR gel would solve these problems and make it possible to test the MR guided Radiotherapy (MRgRT) in 3D. By scanning and irradiating at the same time, it could be possible to follow the dose distribution real-time. In this way, the dose could be evaluated during delivery. Imaging the phantom in-situ would eliminate phantom setup uncertainty from the end-to-end test. In the sections below, how to perform the end-to-end test is described in the section Methods and Materials. The discussion section includes comments on relative and absolute dosimetry , as well as the MR sequence to use and real-time dosimetry. This is followed by the conclusion. Unfortunately, due to the corona crisis, it was not possible to conduct the experiment.

6.2 Methods and materials

For this experiment, the Prime phantom from RTSafe would be used. This is an anthropomorphic, inhomogeneous head phantom based on an actual patient's CT scan. Different dosimetry inserts can be placed in the phantom, for example an ion chamber, TLD's, film or gel. The phantom is shown in figure 32. For this experiment, an end-to-end test will be done using film, an ionization chamber and gel. In this way it will be possible to compare the dosimetry methods with each other.

Figure 32: The Prime phantom from RTSafe with all possible inserts. [57]

The first step for this end-to-end test is to acquire CT scans of the phantom in each of the three configurations. A treatment plan is then made for the

CT of the phantom with the gel, according to local protocol. For the other two phantom configurations, the same treatment plan is used. For this end-to-end test, a stereotactic brain metastasis plan is made. A dose of 21 Gy is planned to a PTV volume between 1 and 10 cm^3. A radiotherapy technician (RTT) does the planning, as is also done in clinical practice. After this, the clinical workflow is followed. The treatment starts with a pre-treatment MRI to verify the location of the phantom, target and any identified organs at risk. With this pre-treatment MRI, the plan is adapted to the current position. This adapted plan is then used to irradiate the phantom with each of the inserts (gel, ionization chamber, film) in turn. The irradiation is then interrupted at a random moment, after which the phantom is moved and a new MRI is made. In this way, also the situation when a patient moves during treatment can be checked. On this new MRI, a new, adapted plan is made. The rest of the new, adapted plan is then irradiated. After irradiation, the dose distributions of the gel and film and the dose measured by the ionization chamber can be compared with each other and with the TPS data. A gamma pass rate can be calculated for the film and the gel. The gel can be read-out after 20-30 minutes up until 1.5 hours after irradiation, because that is when the linearity of R2 versus dose is at its highest. For the three methods, the measured dose is compared. For the ionization chamber, the measured electric charge is converted to dose with a calibration factor derived from a 10x10 cm^2 beam, the film is scanned and with an optical density (OD) to dose curve converted to dose. For gel, the R2 has to be converted to dose. There is no fixed conversion from R2 to dose, as can be seen in experiment 2. Therefore, relative dosimetry is done. The normalization point should be in a region of homogeneous high dose in the Planning Target Volume (PTV). For relative dosimetry a gel which did not receive dose should also be scanned, either in the phantom or in a separate vial. In this way, the offset can be determined. If the time dependency of the gel is known, a scan pre-irradiation can be used for this. The results are analyzed with self-written tools in Matlab.

6.3 Discussion

6.3.1 Relative and absolute dosimetry for gels

Relative dosimetry For relative dosimetry, it is needed to know the R2 offset of the gel at the time of measurement. If the offset is known, a relative distribution between 0% and 100% of the maximum measured dose or as percentage of the dose at a of a well-identified point such as an ionization chamber or isocenter can be made. To see if the offset would change with MR sequence, the offset was analyzed for the three sequences used in experiment 2. The results are shown in figure 33. This figure shows that the offset is not the same for each sequence. This means that, if a new sequence is developed, the R2-offset as a function of time after irradiation should be determined again. Besides this, it should also be checked that the time-dependent offset does not change with a different gel batch, so the experiment should be repeated. The offset does not only change after irradiation, the R2 also changes gradually without irradiation. Therefore, it might be possible to use an unirradiated vial to determine the offset. However, it is important to take the time between production of the gel and irradiation into account and thus, the unirradiated vial should be scanned

at approximately the same time as the phantom. Another option would be to use a part of the gel which receives 0 Gy to determine the offset.

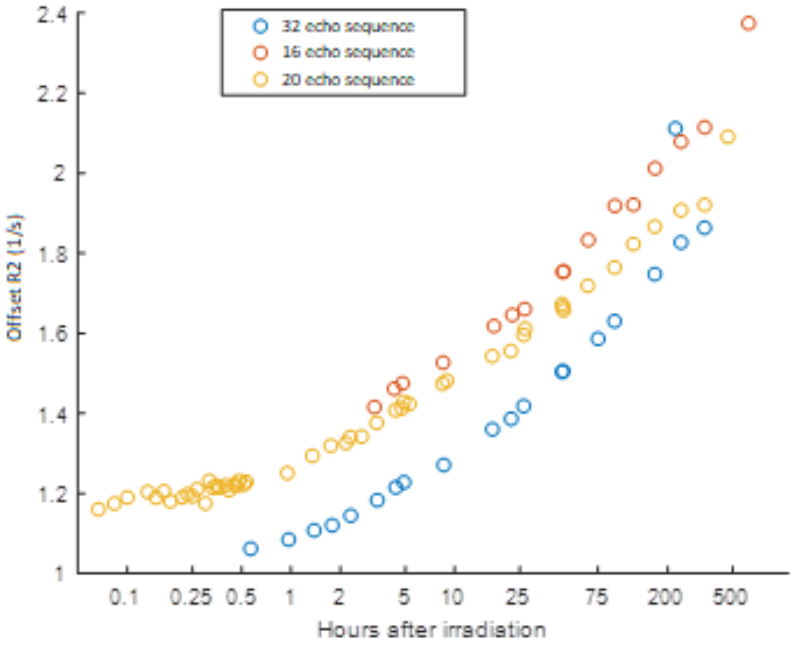

Figure 33: The R2 offset over time for three different sequences. The behavior of the offset is the same for each sequence, but the absolute value is different.

Absolute dosimetry To be able to do absolute dosimetry with gels, a T2 or R2 value should be converted to dose. If the measured R2 at a certain point in time for a specific dose is the same for each batch of gels, no extra calibration is needed. To check this, experiment 2 should be repeated to see if the same curves originate. This was not done for this project. As first investigation, the results from experiment 1 and 2 were compared, which used gels from different batches. In both experiments, doses of 4 and 8 Gy were irradiated. The vials were scanned with different MR sequences and different MR scanners, but they are both scanned with 20 echo sequences and with 32 echo sequences. The results from both experiments are shown in figure 34. If the results from the first experiment are plotted versus the time on a log scale, it is also possible to make a linear fit for those results. The fits for the first experiment can also be compared to the fits for the second experiment (after 7 hours). The results for the fits are shown in tables 7 and 8. It can be seen in the figures that the vials do have the same behavior, and around the same T2 values. To calculate an error, the T2 values from the second experiment were calculated with the fit at the times the scans were made for the first experiment. Those calculated T2 values of experiment 2 were compared to the measured T2 values in experiment

1. The average difference was 3.8%, with a maximum error of 8.5%. From these results, it can not be concluded that a certain T2 or R2 value in time relates to a certain dose. To obtain a more definitive conclusion, experiment 2 should be repeated. The difference might also be caused by the larger uncertainty in dose in experiment 1.

Another option to make absolute dosimetry possible would be to use extra calibration vials. At least two vials from the same batch should be irradiated up to known doses, to make a R2 versus dose curve. Those vials should be read-out via the same sequence as the end-to-end phantom. The time interval between irradiation and scanning should be the same and difference between manufacturing and irradiation of the gel should be taken into account.

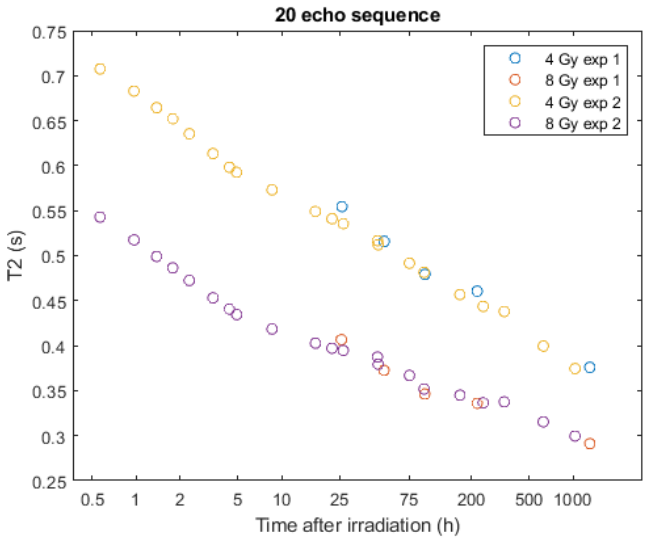

(a)

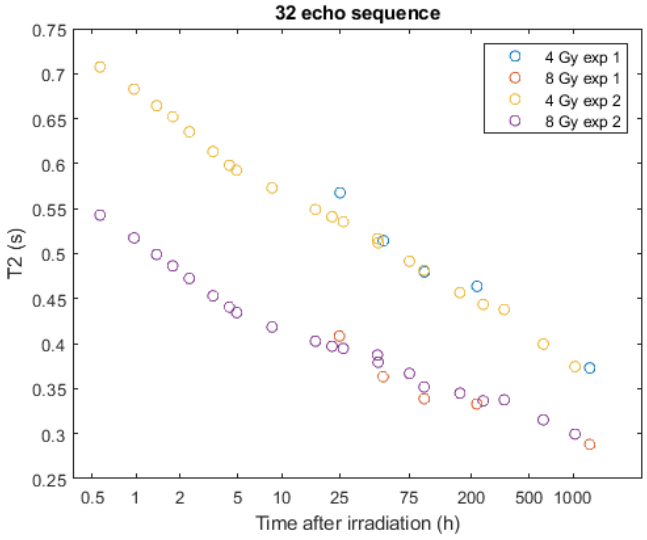

(b)

Figure 34: The combined results from experiments 1 and 2 (a) Vials scanned with the 20 echo sequences (b) Vials scanned with the 32 echo sequences. T2 values for experiment 1 were corrected for the dose measured with the reference vial.

Table 7: Fits for the 20 echo sequences for experiment 1 and 2. Slope (a) and offset (b) of experiment 1 are different than the slope and offset of experiment 2.

	exp1		exp2	
	a	b	a	b
4 Gy	-0.04405	0.6913	-0.03101	0.6171
8 Gy	-0.02771	0.485	-0.0213	0.4684

Table 8: Fits for the 32 echo sequences for experiment 1 and 2. Slope (a) and offset (b) of experiment 1 are different than the slope and offset of experiment 2.

	exp1		exp2	
	a	b	a	b
4 Gy	-0.04651	0.7052	-0.0413	0.6686
8 Gy	-0.02763	0.4801	-0.0247	0.4736

6.3.2 MR sequence and real-time dosimetry

MR sequence The sequence used for experiment 2 is a sequence with 20 echoes with a resolution of 2x2x4 mm^3. This resolution is good enough for uniform dose distributions such as that in experiment 2, but for plan QA, the resolution should be higher. Therefore, a new MR sequence with better spatial resolution should be developed. This sequence should also scan a larger area than in experiment 2, since the whole head phantom should be scanned now. The increase in area and in resolution will cause the sequence to take longer. This gives new problems with the read-out of the gel. If the gel is read-out quickly after irradiation, the T2 at the start of the sequence might be very different from the T2 at the end of the sequence. Therefore, it might be needed to extend the time between irradiation and scanning, depending on how long the sequence takes. With a new sequence, the optimal read-out time might also be different.

Real-time dosimetry For real-time dosimetry, a very fast sequence is needed. It is currently not possible to create a sequence which scans the whole 3D volume with high resolution within seconds, so therefore, real-time dosimetry of the whole volume is not possible. It might however can then be possible to scan only one or two planes. Real-time dosimetry can than be done for these planes, but this does mean that gel dosimetry becomes 2D dosimetry instead of 3D dosimetry. To do 3D dosimetry, the gel should be read-out again after a longer time. If a sequence is made with a duration comparable to the sequence of experiment 2 (1 minute and 12 seconds) or shorter, intra-fraction dosimetry with reasonable errors would be possible. The largest error seen in experiment 2 was about 4%. This is a conservative over-estimate because of the in-exact intra-fraction dose and time determination, and relatively long sequence duration.

6.4 Conclusions

A relative end-to-end test with MR scans after approximately 8 hours is currently most achievable. An area which received 0 Gy can be used to determine the offset and after 8 hours the sensitivity is at its maximum. A new sequence should be developed which scans a larger volume at a higher resolution. This sequence can be used to read-out the phantom. With this new sequence, the optimal read-out time might be changed. The optimal time to read-out the phantom should be determined by repeating experiment 2 with this new sequence. There is more work that needs to be done to make absolute dosimetry possible. There are two ways to do absolute dosimetry. The first one is by irradiating reference vials up to known doses to create an absolute dose calibration curve that is specific for that batch of gel and time. The second method requires a batch-independent time dependency curve. To see if this is achievable, experiment 2 should be repeated with the new sequence at least twice with different batches of gel. Real-time dosimetry is not possible for the whole volume, because of the duration of the sequence. It might be possible to do real-time dosimetry in a plane.

7 Future research

A new MR sequence is required. This MR sequence should have a high spatial resolution and should scan the whole phantom volume. The sequence should be as short as possible, to diminish differences in T2 read-out at the start and the end of the sequence. Ideally, a sequence of only a few seconds would be developed to make real-time dosimetry possible. The geometrical accuracy should also be confirmed for the new MR sequence.

The first performance of an experiment is useful in terms of the acquisition of new data and insight. However the time-dependency experiment performed here must be repeated. A key question is, is the observed time dependency gel batch-specific, or can a model be created that is generally applicable? This should also be done with the newly developed MR sequence. Multiple independent T2 measurements should also be made at the same time point, to determine the uncertainty of the process, and whether accurate absolute dosimetry can be performed. This should be done after at least one day, so that the time between consecutive scans is not influencing the measured T2 too much.

Next, the experiment described in chapter 6 could be carried out. The comparison between film, ionization chamber and gel can then be made. An estimate of the uncertainties can then be given. Efforts should also be made to make 4D dosimetry possible. This requires a very fast MR sequence. If this is not possible for the whole volume, it might be possible to do it for two perpendicular planes.

If the T2 versus time curve is the same for a different gel batch, then a calibration curve could be made for absolute dosimetry. It is also possible to achieve absolute dosimetry using an existing system (e.g. ionization chamber or film). These could also be used for relative dosimetry checks of the gel performance, and to determine the uncertainty of gel dosimetry.

8 Summary

This thesis explored the use of gels for 3D dosimetry in a MR-linac. 3D gel dosimetry can be used for end-to-end testing to test the whole clinical workflow of a MR-linac. It was concluded that the magnetic field did not influence the behavior of the gel. There were no statistically significant differences between the R2 values measured for each magnetic field strength. Thus, as with relative dosimetry in conventional systems, the R2 values were proportional to the delivered dose. Therefore, the VIPAR gel can be used for dosimetry in a MR-linac.

This study provides data on the short-term time dependence of VIPAR gels. There are two chemical processes, which were seen in the data. The data could be fitted with two fits, the first fit included the time points up to 7 hours, the second fit included all time points after 7 hours. The fits can be used to correct for time differences. It was also shown that the sensitivity of the gel is sufficiently high that it can be scanned immediately after irradiation. This is important, because then it is possible to scan the phantom in the treatment position, which is ideal for assessing the positional accuracy of the dose delivery. Maximum sensitivity occurs 7 hours after irradiation and remains stable for at least 43 days, meaning that gels could be scanned, or rescanned at a later date if needed.

An end-to-end test was also designed. A relative end-to-end test with read-out after several hours seems achievable. To read-out the gel quicker after irradiation might be possible, but depends on a fast MR sequence being developed. Real-time dosimetry for the whole volume is not possible currently, because the MR sequence would be to slow. Real-time dosimetry for one or two planes is probably possible. Absolute dosimetry requires an extra calibration with gel, an ionization chamber or film.

References

[1] "Nederlandse Kankerregistratie (NKR), IKNL." Retrieved March 14, 2019, from https://www.cijfersoverkanker.nl/selecties/Dataset_2/img5c8a5ebf0d620.

[2] G. Delaney, S. Jacob, C. Featherstone, and M. Barton, "The role of radiotherapy in cancer treatment: Estimating optimal utilization from a review of evidence-based clinical guidelines," Cancer, vol. 104, no. 6, pp. 1129–1137, 2005.

[3] M. Miften et al., "Tolerance limits and methodologies for IMRT measurement-based verification QA: Recommendations of AAPM Task Group No. 218," Medical Physics, vol. 45, no. 4, pp. e53–e83, 2018.

[4] P. Y. Guo, J. A. Adamovics, and M. Oldham, "Characterization of a new radiochromic three-dimensional dosimeter," Medical Physics, vol. 33, no. 5, pp. 1338–1345, 2006.

[5] T. Gorjiara et al., "Investigation of radiological properties and water equivalency of PRESAGE® dosimeters," Medical Physics, vol. 38, no. 4, pp. 2265–2274, 2011.

[6] G. S. Ibbott, "Applications of gel dosimetry," Journal of Physics: Conference Series, vol. 3, pp. 58–77, 2004.

[7] B. W. Raaijmakers et al., "First patients treated with a 1.5 T MRI-Linac: Clinical proof of concept of a high-precision, high-field MRI guided radiotherapy treatment," Phys. Med. Biol., vol. 62, no. 23, pp. L41–L50, 2017.

[8] M. J. Day and G. Stein, "Chemical effects of ionizing radiation in some gels," Nature, vol. 166, no. 4212. pp. 146–147, 1950.

[9] J. C. Gore and Y. S. Kang, "Measurement of radiation dose distributions by nuclear magnetic resonance (NMR) imaging," Physics in Medicine and Biology, vol. 29, no. 10, pp. 1189–1197, 1984.

[10] Baldock et al., "Polymer gel dosimetry," Physics in Medicine and Biology, vol. 55, no. 5, pp. R1–R63, 2010.

[11] G. S. Ibbott, "Gel dosimetry," Journal of the American College of Radiology, vol. 3, no. 2, pp. 144–146, 2006.

[12] M. J. Maryanski, J. C. Gore, R. P. Kennan, and R. J. Schulz, "NMR relaxation enhancement in gels polymerized and cross-linked by ionizing radiation: A new approach to 3D dosimetry by MRI," Magnetic Resonance Imaging, vol. 11, no. 2, pp. 253–258, 1993.

[13] P. Kipouros et al., "Wide dynamic dose range of VIPAR polymer gel dosimetry," Physics in Medicine and Biology, vol. 46, no. 8, pp. 2143–2159, 2001.

[14] Y. De Deene et al., "A basic study of some normoxic polymer gel dosimeters," Physics in Medicine and Biology, vol. 47, no. 19, pp. 3441–3463, Oct. 2002.

[15] B. Farhood, G. Geraily, and S. M. M. Abtahi, "A systematic review of clinical applications of polymer gel dosimeters in radiotherapy," Applied Radiation and Isotopes, vol. 143, no. February 2018, pp. 47–59, 2019.

[16] H. Fricke and E. Hart, "The chemical action of roentgen rays on dilute ferrosulphate solutions as a measure of dose," The American Journal of Roentgenology Radium Therapy and Nuclear Medicine, vol. 18, pp. 430–432, 1927.

[17] L. J. Schreiner, "Review of Fricke gel dosimeters," Journal of Physics: Conference Series, vol. 3, pp. 9–21, 2004.

[18] Y. S. Soliman, M. I. El Gohary, M. H. Abdel Gawad, E. A. Amin, and O. S. Desouky, "Fricke gel dosimeter as a tool in quality assurance of the radiotherapy treatment plans," International Journal of Applied Radiation and Isotopes, vol. 120, no. December 2016, pp. 126–132, 2017.

[19] P. Alexander, A. Charlesby, and M. Ross, "The degradation of solid polymethylmethacrylate by ionizing radiation," Proceedings of the Royal Society of London. Series A, Mathematical and Physical Sciences, vol. 223, no. 1154, pp. 392–404, May 1954.

[20] F. E. Hoecker and I. W. Watkins, "Radiation polymerization dosimetry," The International Journal of Applied Radiation and Isotopes, vol. 3, no. 1, pp. 31–35, Jan. 1958.

[21] A. L. Boni, "A Polyacrylamide Gamma Dosimeter," Journal of Radiation Research, vol. 14, no. 4, p. 374, Apr. 1961.

[22] M. Maryanski, J. Gore, ... R. S.-. I. S. for M. R. in M., and U. 1992, "3-D radiation dosimetry by MRI: solvent proton relaxation enhancement by radiation-controlled polymerisation and cross-linking in gels," Proceedings of the International Society for Magnetic Resonance in Medicine (New York), 1992.

[23] M. J. Maryanski et al., "Magnetic resonance imaging of radiation dose distributions using a polymer-gel dosimeter," Physics in Medicine and Biology, vol. 39, no. 9, pp. 1437–1455, 1994.

[24] M. Hilts, A. Jirasek, and C. Duzenli, "Effects of gel composition on the radiation induced density change in PAG polymer gel dosimeters: A model and experimental investigations," Physics in Medicine and Biology, vol. 49, no. 12, pp. 2477–2490, Jun. 2004.

[25] C. Baldock et al., "Experimental procedure for the manufacture and calibration of polyacrylamide gel (PAG) for magnetic resonance imaging (MRI) radiation dosimetry," Physics in Medicine and Biology, vol. 43, no. 3. pp. 695–702, 1998.

[26] M. Khan, G. Heilemann, P. Kuess, D. Georg, and A. Berg, "The impact of the oxygen scavenger on the dose-rate dependence and dose sensitivity of MAGIC type polymer gels," Physics in Medicine and Biology, vol. 63, p. 12, 2018.

[27] E. Pappas et al., "A new polymer gel for magnetic resonance imaging (MRI) radiation dosimetry," Physics in Medicine and Biology, vol. 44, no. 10, pp. 2677–2684, 1999.

[28] J. C. Gore, M. Ranade, M. J. Maryañski, and R. J. Schulz, "Radiation dose distributions in three dimensions from tomographic optical density scanning of polymer gels: I. Development of an optical scanner," Physics in Medicine and Biology, vol. 41, no. 12, pp. 2695–2704, 1996.

[29] S. M. Abtahi, S. M. R. Aghamiri, and H. Khalafi, "Optical and MRI investigations of an optimized acrylamide-based polymer gel dosimeter," Journal of Radioanalytical and Nuclear Chemistry, vol. 300, no. 1, pp. 287–301, 2014

[30] J. V Trapp, G. Michael, Y. De Deene, and C. Baldock, "Attenuation of diagnostic energy photons by polymer gel dosimeters," Physics in Medicine and Biology, vol. 47, pp. 4247–4258, 2002.

[31] M. L. Mather, A. K. Whittaker, and C. Baldock, "Ultrasound evaluation of polymer gel dosimeters Ultrasound evaluation of polymer gel dosimeters," Physics in Medicine and Biology, vol. 47, pp. 1449–1458, 2002.

[32] C. Baldock, L. Rintoul, S. F. Keevil, J. M. Pope, and G. A. George, "Fourier transform Raman spectroscopy of polyacrylamide gels (PAGs) for radiation dosimetry," Physics in Medicine and Biology, vol. 43, pp. 3617–3627, 1998.

[33] Brown, R. W., Cheng, Y.-C., Haacke, E. M., Thompson, M. R., and Venkatesan, R. (2014). Magnetic Resonance Imaging: Physical Principles and Sequence Design.

[34] Y. De Deene, P. Hanselaer, C. De Wagter, E. Achten, and W. De Neve, "An investigation of the chemical stability of a monomer / polymer gel dosimeter," Physics in Medicine and Biology, vol. 45, pp. 859–878, 2000.

[35] M. Papoutsaki, T. G. Maris, and E. Pappas, "Dosimetric characteristics of a new polymer gel and their dependence on post-preparation and post-irradiation time: Effect on X-ray beam profile measurements," Physica Medica, no. 29, pp. 453–460, 2013.

[36] Y. De Deene, K. Vergote, C. Claeys, and C. De Wagter, "The fundamental radiation properties of normoxic polymer gel dosimeters: a comparison between a methacrylic acid based gel and acrylamide based gels ," Physics in Medicine and Biology, vol. 51, 653–673, 2006.

[37] M. Kozicki, M. Jaszczak, P. Maras, M. Dudek, and M. Cłapa, "On the development of a VIPAR nd radiotherapy 3D polymer gel dosimeter," Phys. Med. Biol., vol. 62, no. 3, pp. 986–1008, 2017.

[38] M. J. Maryanski, C. Audet, and J. C. Gore, "Effects of crosslinking and temperature on the dose response of a BANG polymer gel dosimeter," Phys. Med. Biol., vol. 42, no. 2, Feb. 1997.

[39] E. Pappas et al., "Narrow stereotactic beam profile measurements using N-vinylpyrrolidone based polymer gels and magnetic resonance imaging," Physics in Medicine and Biology, vol. 46, no. 3, pp. 783–797, 2001.

[40] E. Pappas, A. Angelopoulos, P. Kipouros, L. Vlachos, S. Xenofos, and I. Seimenis, "Evaluation of the performance of VIPAR polymer gels using a variety of x-ray and electron beams," Physics in Medicine and Biology, vol. 48, no. 5, 2003.

[41] D. Saenz et al., "QA for SBRT of Spine Lesions: Introducing a Novel 3D Gel Dosimeter for Spatial and Dosimetric End-to-End Testing," International Journal of Radiation Oncology, vol. 102, no. 3, p. e517, Nov. 2018.

[42] H. Liu et al., "Dosimetric validation for an automatic brain metastases planning software using single-isocenter dynamic conformal arcsDosimetric validation for an automatic brain metastases planning software using single-isocenter dynamic conformal arcs," Journal of Applied Clinical Medical Physics, vol. 17, no. 5, p. 6320, 2016.

[43] A. J. E. Raaijmakers, B. W. Raaymakers, and J. J. W. Lagendijk, "Integrating a MRI scanner with a 6 MV radiotherapy accelerator: Dose increase at tissue-air interfaces in a lateral magnetic field due to returning electrons," Physics in Medicine and Biology, vol. 50, no. 7, pp. 1363–1376, 2005.

[44] J. J. W. Lagendijk et al., "MRI/linac integration," Radiotherapy and Oncology, vol. 86, no. 1, pp. 25–29, 2008.

[45] A. J. E. Raaijmakers, B. W. Raaymakers, and J. J. W. Lagendijk, "Magnetic-field-induced dose effects in MR-guided radiotherapy systems: Dependence on the magnetic field strength," Physics in Medicine and Biology, vol. 53, no. 4, pp. 909–923, 2008.

[46] A. J. E. Raaijmakers, B. W. Raaymakers, S. Van Der Meer, and J. J. W. Lagendijk, "Integrating a MRI scanner with a 6 MV radiotherapy accelerator: Impact of the surface orientation on the entrance and exit dose due to the transverse magnetic field," Physics in Medicine and Biology, vol. 52, no. 4, pp. 929–939, 2007.

[47] H. J. Lee, M. Kadbi, G. Bosco, and G. S. Ibbott, "Real-time volumetric relative dosimetry for magnetic resonance - Image-guided radiation therapy (MR-IGRT)," Physics in Medicine and Biology, vol. 63, no. 4, 2018.

[48] Y. Roed, L. Pinsky, and G. Ibbott, "Polymer gel dosimetry in the presence of a strong magnetic field," Journal of Physics: Conference Series, vol. 1305, p. 012014, 2019.

[49] B. Loughery et al., "Multi-institutional evaluation of end-to-end protocol for IMRT/VMAT treatment chains utilizing conventional linacs," Medical Dosimetry, vol. 44, no. 1, pp. 61–66, 2019

[50] L. Tuntipumiamorn et al., "Multi-institutional evaluation using the end-to-end test for implementation of dynamic techniques of radiation therapy in Thailand," Reports of Practical Oncology and Radiotherapy, vol. 24, no. 1, pp. 124–132, 2019.

[51] D. Hoffmans, N. Niebuhr, O. Bohoudi, A. Pfaffenberger, and M. Palacios, "An end-to-end test for MR-guided online adaptive radiotherapy," Physics in Medicine and Biology, in press, 2020.

[52] A. Elter et al., "End-to-end test of an online adaptive treatment procedure in MR-guided radiotherapy using a phantom with anthropomorphic structures," Physics in Medicine and Biology, vol. 64, no. 22, 2019.

[53] J. Daniel Bourland, "Radiation Oncology Physics," in Clinical Radiation Oncology: Third Edition, Elsevier Inc., 2011, pp. 95–152.

[54] P. K. Kim et al., "Myocardial T1 and T2 mapping: Techniques and clinical applications," Korean Journal of Radiology, vol. 18, no. 1. Korean Radiological Society, pp. 113–131, 01-Jan-2017.

[55] A. S. Lota, P. D. Gatehouse, and R. H. Mohiaddin, "T2 mapping and T2* imaging in heart failure," Heart Failure Reviews, vol. 22, no. 4. Springer New York LLC, pp. 431–440, 01-Jul-2017.

[56] Milford, D., Rosbach, N., Bendszus, M., and Heiland, S. (2015). Monoexponential fitting in T2-relaxometry: Relevance of offset and first echo. PLoS ONE, 10(12), 1–13.

[57] "RTSafe product catalogus." [Online]. Available: https://rtsafe.com/media/content/product_catalogdocument_files/RTSAFE_PRODUCT_CATALOG_2020.pdf. [Accessed: 01-May-2020].